2 **Kiyosawa K**, Sodeyama T, Tanaka E, Gibo Y, Yoshizawa K, Nakano Y, Furuta S, Akahane Y, Nishioka K, Purcell RH. Interrelationship of blood transfusion, non-A, non-B hepatitis and hepatocellular carcinoma: analysis by detection of antibody to hepatitis C virus. *Hepatology* 1990; **12**: 671-675 [PMID: 2170265]

3 **Major ME**, Feinstone SM. The molecular virology of hepatitis C. *Hepatology* 1997; **25**: 1527-1538 [PMID: 9185778]

4 **Ogata N**, Alter HJ, Miller RH, Purcell RH. Nucleotide sequence and mutation rate of the H strain of hepatitis C virus. *Proc Natl Acad Sci USA* 1991; **88**: 3392-3396 [PMID: 1849654]

5 **Kurosaki M**, Enomoto N, Marumo F, Sato C. Rapid sequence variation of the hypervariable region of hepatitis C virus during the course of chronic infection. *Hepatology* 1993; **18**: 1293-1299 [PMID: 8244252]

6 **Martell M**, Esteban JI, Quer J, Genescà J, Weiner A, Esteban R, Guardia J, Gómez J. Hepatitis C virus (HCV) circulates as a population of different but closely related genomes: quasispecies nature of HCV genome distribution. *J Virol* 1992; **66**: 3225-3229 [PMID: 1313927]

7 **Saito T**, Watanabe H, Shao L, Okumoto K, Hattori E, Sanjo M, Misawa K, Suzuki A, Takeda T, Sugahara K, Ito JI, Saito K, Togashi H, Kawata S. Transmission of hepatitis C virus quasispecies between human adults. *Hepatol Res* 2004; **30**: 57-62 [PMID: 15519268]

8 **Liu CH**, Chen BF, Chen SC, Lai MY, Kao JH, Chen DS. Selective transmission of hepatitis C virus quasi species through a needlestick accident in acute resolving hepatitis. *Clin Infect Dis* 2006; **42**: 1254-1259 [PMID: 16586384]

9 **Sulkowski MS**, Ray SC, Thomas DL. Needlestick transmission of hepatitis C. *JAMA* 2002; **287**: 2406-2413 [PMID: 11988061]

10 **Mizuno Y**, Suzuki K, Mori M, Hayashi K, Owaki T, Hayashi H, Kumada K, Ohba K, Mizokami M. Study of needlestick accidents and hepatitis C virus infection in healthcare workers by molecular evolutionary analysis. *J Hosp Infect* 1997; **35**: 149-154 [PMID: 9049819]

11 **Frijstein G**, Hortensius J, Zaaijer HL. Needlestick injuries and infectious patients in a major academic medical centre from 2003 to 2010. *Neth J Med* 2011; **69**: 465-468 [PMID: 22058270]

12 **Suzuki K**, Mizokami M, Lau JY, Mizoguchi N, Kato K, Mizuno Y, Sodeyama T, Kiyosawa K, Gojobori T. Confirmation of hepatitis C virus transmission through needlestick accidents by molecular evolutionary analysis. *J Infect Dis* 1994; **170**: 1575-1578 [PMID: 7527827]

13 **Omata M**, Yokosuka O, Takano S, Kato N, Hosoda K, Imazeki F, Tada M, Ito Y, Ohto M. Resolution of acute hepatitis C after therapy with natural beta interferon. *Lancet* 1991; **338**: 914-915 [PMID: 1681268]

14 **Sharland M**, Patton MA, Hill L. Ectrodactyly of hands and feet in a child with a complex translocation including 7q21.2. *Am J Med Genet* 1991; **39**: 413-414 [PMID: 1877619 DOI: 10.1093/jac/dkn346]

15 **Fabrizi F**, Dixit V, Messa P, Martin P. Interferon therapy of acute hepatitis C in dialysis patients: meta-analysis. *J Viral Hepat* 2012; **19**: 784-791 [PMID: 23043385 DOI: 10.1111/j.1365-2893.2012.01607.x]

16 **Nunnari G**, Montineri A, Portelli V, Savalli F, Fatuzzo F, Cacopardo B. The use of peginterferon in monotherapy or in combination with ribavirin for the treatment of acute hepatitis C. *Eur Rev Med Pharmacol Sci* 2012; **16**: 1013-1016 [PMID: 22913149]

17 **Farci P**, Munoz SJ, Shimoda A, Govindarajan S, Wong DC, Coiana A, Peddis G, Rubin R, Purcell RH. Experimental transmission of hepatitis C virus-associated fulminant hepatitis to a chimpanzee. *J Infect Dis* 1999; **179**: 1007-1011 [PMID: 10068599]

18 **Di Bisceglie AM**. Natural history of hepatitis C: its impact on clinical management. *Hepatology* 2000; **31**: 1014-1018 [PMID: 10733560]

19 **Gerlach JT**, Diepolder HM, Zachoval R, Gruener NH, Jung MC, Ulsenheimer A, Schraut WW, Schirren CA, Waechtler M, Backmund M, Pape GR. Acute hepatitis C: high rate of both spontaneous and treatment-induced viral clearance. *Gastroenterology* 2003; **125**: 80-88 [PMID: 12851873]

20 **Micallef JM**, Kaldor JM, Dore GJ. Spontaneous viral clearance following acute hepatitis C infection: a systematic review of longitudinal studies. *J Viral Hepat* 2006; **13**: 34-41 [PMID: 16364080]

21 **Ishibashi M**, Shinzawa H, Kuboki M, Tsuchida H, Takahashi T. Prevalence of inhabitants with anti-hepatitis C virus antibody in an area following an acute hepatitis C epidemic: age-and area-related features. *J Epidemiol* 1996; **6**: 1-7 [PMID: 8795951]

22 **Saito T**, Ji G, Shinzawa H, Okumoto K, Hattori E, Adachi T, Takeda T, Sugahara K, Ito JI, Watanabe H, Saito K, Togashi H, Ishii K, Matsuura T, Inageda K, Muramatsu M, Kawata S. Genetic variations in humans associated with differences in the course of hepatitis C. *Biochem Biophys Res Commun* 2004; **317**: 335-341 [PMID: 15063762]

23 **Farci P**, Shimoda A, Coiana A, Diaz G, Peddis G, Melpolder JC, Strazzera A, Chien DY, Munoz SJ, Balestrieri A, Purcell RH, Alter HJ. The outcome of acute hepatitis C predicted by the evolution of the viral quasispecies. *Science* 2000; **288**: 339-344 [PMID: 10764648]

24 **Liu L**, Fisher BE, Thomas DL, Cox AL, Ray SC. Spontaneous clearance of primary acute hepatitis C virus infection correlated with high initial viral RNA level and rapid HVR1 evolution. *Hepatology* 2012; **55**: 1684-1691 [PMID: 22234804 DOI: 10.1002/hep.25575]

25 **Khakoo SI**, Thio CL, Martin MP, Brooks CR, Gao X, Astemborski J, Cheng J, Goedert JJ, Vlahov D, Hilgartner M, Cox S, Little AM, Alexander GJ, Cramp ME, O'Brien SJ, Rosenberg WM, Thomas DL, Carrington M. HLA and NK cell inhibitory receptor genes in resolving hepatitis C virus infection. *Science* 2004; **305**: 872-874 [PMID: 15297676]

26 **Watanabe H**, Saito T, Shinzawa H, Okumoto K, Hattori E, Adachi T, Takeda T, Sugahara K, Ito JI, Saito K, Togashi H, Suzuki R, Hayashi M, Miyamura T, Matsuura Y, Kawata S. Spontaneous elimination of serum hepatitis C virus (HCV) RNA in chronic HCV carriers: a population-based cohort study. *J Med Virol* 2003; **71**: 56-61 [PMID: 12858409]

27 **Rehermann B**, Nascimbeni M. Immunology of hepatitis B virus and hepatitis C virus infection. *Nat Rev Immunol* 2005; **5**: 215-229 [PMID: 15738952]

28 **Kimura T**, Saito T, Yoshimura M, Yixuan S, Baba M, Ji G, Muramatsu M, Kawata S. Association of transforming growth factor-beta 1 functional polymorphisms with natural clearance of hepatitis C virus. *J Infect Dis* 2006; **193**: 1371-1374 [PMID: 16619184]

29 **Ge D**, Fellay J, Thompson AJ, Simon JS, Shianna KV, Urban TJ, Heinzen EL, Qiu P, Bertelsen AH, Muir AJ, Sulkowski M, McHutchison JG, Goldstein DB. Genetic variation in IL28B predicts hepatitis C treatment-induced viral clearance. *Nature* 2009; **461**: 399-401 [PMID: 19684573 DOI: 10.1038/nature08309]

30 **Tanaka Y**, Nishida N, Sugiyama M, Kurosaki M, Matsuura K, Sakamoto N, Nakagawa M, Korenaga M, Hino K, Hige S, Ito Y, Mita E, Tanaka E, Mochida S, Murawaki Y, Honda M, Sakai A, Hiasa Y, Nishiguchi S, Koike A, Sakaida I, Imamura M, Ito K, Yano K, Masaki N, Sugauchi F, Izumi N, Tokunaga K, Mizokami M. Genome-wide association of IL28B with response to pegylated interferon-alpha and ribavirin therapy for chronic hepatitis C. *Nat Genet* 2009; **41**: 1105-1109 [PMID: 19749757 DOI: 10.1038/ng.449]

31 **Balagopal A**, Thomas DL, Thio CL. IL28B and the control of hepatitis C virus infection. *Gastroenterology* 2010; **139**: 1865-1876 [PMID: 20950615 DOI: 10.1053/j.gastro.2010.10.004]

32 **Thomas DL**, Thio CL, Martin MP, Qi Y, Ge D, O'Huigin C, Kidd J, Kidd K, Khakoo SI, Alexander G, Goedert JJ, Kirk GD, Donfield SM, Rosen HR, Tobler LH, Busch MP, McHutchison JG, Goldstein DB, Carrington M. Genetic variation in IL28B and spontaneous clearance of hepatitis C virus. *Nature* 2009; **461**: 798-801 [PMID: 19759533 DOI: 10.1038/nature08463]

33 **Hung CH**, Chang KC, Lu SN, Wang JH, Chen CH, Lee CM, Hu TH. Spontaneous clearance of hepatitis C virus in an interleukin 28B favorable genotype highly prevalent area. *Hepatology* 2013; **57**: 2089-2090 [PMID: 22886694 DOI: 10.1002/hep.26002]

34 **Duggal P**, Thio CL, Wojcik GL, Goedert JJ, Mangia A, Latanich R, Kim AY, Lauer GM, Chung RT, Peters MG, Kirk GD, Mehta SH, Cox AL, Khakoo SI, Alric L, Cramp ME, Donfield SM, Edlin BR, Tobler LH, Busch MP, Alexander G, Rosen HR, Gao X, Abdel-Hamid M, Apps R, Carrington M, Thomas DL. Genome-wide association study of spontaneous resolution of hepatitis C virus infection: data from multiple cohorts. *Ann Intern Med* 2013; **158**: 235-245 [PMID: 23420232 DOI: 10.7326/0003-4819-158-4-201302190-00003]

35 **Mangia A**, Santoro R, Copetti M, Massari M, Piazzolla V, Spada E, Cappucci G, Missale G, Mottola L, Agostinacchio E, Mauro Ld, Zuccaro O, Maio P, Pellegrini F, Folgori A, Ferrari C. Treatment optimization and prediction of HCV clearance in patients with acute HCV infection. *J Hepatol* 2013; **59**: 221-228 [PMID: 23587473 DOI: 10.1016/j.jhep.2013.04.007]

36 **Prokunina-Olsson L**, Muchmore B, Tang W, Pfeiffer RM, Park H, Dickensheets H, Hergott D, Porter-Gill P, Mumy A, Kohaar I, Chen S, Brand N, Tarway M, Liu L, Sheikh F, Astemborski J, Bonkovsky HL, Edlin BR, Howell CD, Morgan TR, Thomas DL, Rehermann B, Donnelly RP, O'Brien TR. A variant upstream of IFNL3 (IL28B) creating a new interferon gene IFNL4 is associated with impaired clearance of hepatitis C virus. *Nat Genet* 2013; **45**: 164-171 [PMID: 23291588 DOI: 10.1038/ng.2521]

P- Reviewers: Koch TR, Roda G, Seicean A **S- Editor**: Ma YJ
L- Editor: Logan S **E- Editor**: Ma S

Clin J Gastroenterol (2014) 7:58–61
DOI 10.1007/s12328-013-0438-2

CASE REPORT

Possible autoimmune hepatitis induced after chronic active Epstein–Barr virus infection

Yoshiko Wada · Chikako Sato · Kyoko Tomita · Rika Ishii-Aso · Hiroaki Haga · Kazuo Okumoto · Yuko Nishise · Hisayoshi Watanabe · Takafumi Saito · Yoshiyuki Ueno

Received: 18 September 2013 / Accepted: 11 November 2013 / Published online: 23 November 2013

Abstract Chronic active Epstein–Barr virus infection (CAEBV) can be manifested in a variety of systemic conditions, including interstitial pneumonia, malignant lymphoma, and coronary aneurysm. Sometimes it may be associated with hepatic failure, although the mechanism underlying CAEBV-related hepatotoxicity remains unclear. We encountered a case of autoimmune hepatitis (AIH) associated with CAEBV. A 61-year-old male was referred to our hospital because of abnormal liver enzyme levels after initial diagnosis of CAEBV had been made by laboratory tests and liver biopsy. On admission, positivity for anti-nuclear antibody was evident, and examination of the liver biopsy specimen showed findings compatible with AIH. Steroid administration was initiated, and the liver function parameters subsequently improved. Although phenotypic changes in liver biopsy specimens are rare in this condition, the present case could provide clues to the possible pathogenesis of AIH.

Keywords Autoimmune hepatitis · Steroids · Anti-nuclear antibody · Epstein–Barr virus

Abbreviations

CAEBV	Chronic active Epstein–Barr virus infection
AIH	Autoimmune hepatitis
ANA	Anti-nuclear antibody

Y. Wada · C. Sato · K. Tomita (✉) · R. Ishii-Aso · H. Haga · K. Okumoto · Y. Nishise · H. Watanabe · T. Saito · Y. Ueno
Department of Gastroenterology, Yamagata University Faculty of Medicine, 2-2-2 Iidanishi, Yamagata 990-9585, Japan
e-mail: to.kyoko@med.id.yamagata-u.ac.jp

Introduction

Chronic active Epstein–Barr virus infection (CAEBV) is a rare condition producing chronic or repeated symptoms mimicking infectious mononucleosis (IM), and an abnormal pattern of anti-EBV antibodies. CAEBV is also known to demonstrate a variety of clinical symptoms, possibly due to an abnormal lymphoproliferative reaction [1]. Accumulation of reported cases has suggested that the prognosis of CAEBV is worse than was originally considered [2, 3]. Although the pathogenesis of CAEBV remains mostly unclear, the source of the EBV-infected cells, and whether they are T cells or natural killer cells appear to be determinants of outcome [4]. CAEBV can cause various forms of liver injury, ranging from simple liver enzyme abnormality to hepatic failure [5].

Autoimmune hepatitis (AIH) is a classical autoimmune liver disease with characteristic clinical manifestations including a female predominance, presence of autoantibodies (especially anti-nuclear antibody; ANA) and hyperimmunoglobulinemia. AIH sometimes presents as an acute form, in which ANA is frequently negative and serum immunoglobulin (Ig) G levels are normal. As is the case for other autoimmune liver diseases, the pathogenesis of AIH is unknown. However, there are a number of possible factors involved in initiation of the abnormal autoimmune reaction in AIH, including a genetic predisposition to exogenous infections.

Here we report a case of AIH that was possibly induced by CAEBV.

Case report

A 61-year-old male was referred to our hospital because of persistent liver enzyme abnormalities and general fatigue.

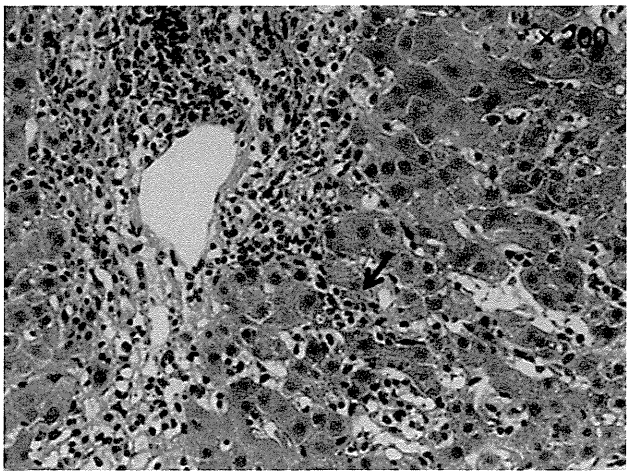

Fig. 1 Initial liver biopsy revealed mononuclear cell infiltration in the sinusoids, suggesting changes after EBV infection

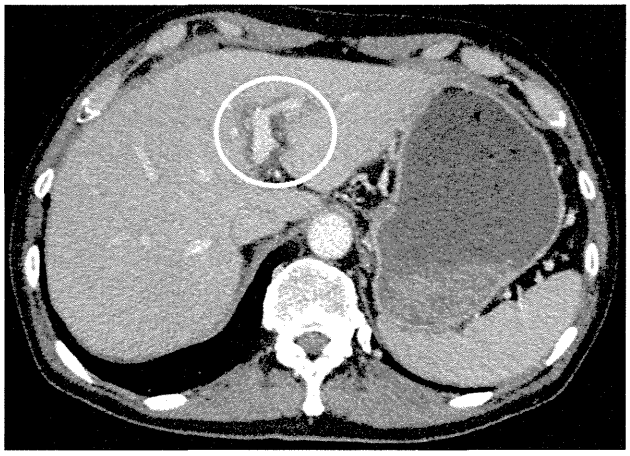

Fig. 2 Hypo-enhanced area reflecting periportal edema and presence of mild hepatosplenomegaly were noted by enhanced abdominal CT scan

Table 1 Laboratory tests on admission to our hospital

T-Bil	2.7 mg/dL	WBC	$3.50 \times 10^3/\mu L$
D-Bil	1.7 mg/dL	Neut	58.3 %
AST	696 IU/L	Lymph	30.5 %
ALT	634 IU/L	Mono	6.0 %
LDH	400 IU/L	Eosino	3.3 %
GGTP	312 IU/L	Baso	1.9 %
ALP	366 IU/L	RBC	$3.80 \times 10^6/\mu L$
TP	7.9 g/dL	Hb	12.4 g/dL
Alb	3.8 g/dL	Platelets	128,000/μL
BUN	11 mg/dL	PT (%)	93 %
Crea	0.54 mg/dL	T-cho	172 mg/dL
Na	140 mEq/L	TG	283 mg/dL
K	4.2 mEq/L	HbA1c	4.6 %
Cl	104 mEq/L	HBsAg	Negative
CRP	0.84 mg/dL	HBsAb	Negative
IgG	2,440 mg/dL	HBcAb	Negative
IgA	331 mg/dL	IgM HAAb	Negative
IgM	107 mg/dL	IgM HBcAb	Negative
AFP	50.6 ng/mL	HCV Ab	Negative
		HIV Ab	Negative
(Urine)		ANA Ab	×320
pH	6.0	Anti-LKM Ab	Negative
Sugar	–	Anti M2 Ab	<5.0 Negative
Protein	–	EBV VCA IgM	Negative
Blood	–	EBV VCA IgG	×2,560
Keton	–	EBNA	×160
Bilirubin	1+	EB EA-DR IgG	×20
		EB EA-DR IgA	<×10
Bone marrow: no atypical cell, no hemophagocytosis		EBV DNA (PCR)[a]	1.3×10^3 copy
		sIL-2 receptor	1,300 IU/mL

[a] EBV monoclonality was negative

His medical history was unremarkable except for rhinosinusitis at 20 years of age and hyperuricemia at 54 years of age. The clinical history of allergy for insect bite was negative. His family history included colon cancer in the father and essential hypertension in the mother. He had been a non-smoker and a moderate drinker (500 mL of beer per day). In December 2010, he had felt general fatigue and visited his family practitioner. Symptoms such as lymphadenopathy and fever were negative except for persistent general fatigue. Clinical laboratory tests revealed liver enzyme abnormalities, and the patient was referred to the community hospital, where CAEBV was initially suspected on the basis of positive peripheral blood EBV DNA with 1.8×10^2 copies/10^6 cells (normal limit $<2.0 \times 10^1$ copies/10^6 cells, by real-time polymerase chain reaction; PCR) [6]. Liver biopsy was performed, and the findings were consistent with liver injury associated with CAEBV (Fig. 1), mainly non-specific mononuclear cell infiltration of the hepatic sinusoids. However, the patient's liver enzymes persistently fluctuated, and therefore he was referred to our hospital in May 2011. Physical examination on admission showed a height of 170.0 cm, body weight 65 kg, body temperature 36.3 °C, blood pressure 124/79 mmHg, clear consciousness, icteric conjunctiva, and hepatomegaly palpable for 2 finger breadths without splenomegaly. No systemic lymph node swelling was evident. The results of laboratory tests on admission are shown in Table 1—these included an elevated transaminase level, a high IgG level, elevated ANA titers (80× to 320×), and a high titer of EBV viral capsid antigen (VCA) IgG. We could not perform HLA-DR genotyping assay with the patient. Imaging (contrast-enhanced computed tomography; CT) revealed a hypo-enhanced area possibly reflecting periportal edema, and mild hepatosplenomegaly (Fig. 2). Positive EBV DNA (1.3×10^3 copies/10^6cells) in

peripheral blood on admission strongly suggested the presence of persistent CAEBV. However, in view of the increased titer of ANA, we performed a second liver biopsy, which revealed fibrous enlargement of the portal area, presence of interfacial hepatitis, and plasma cell-predominant infiltration, thus supporting a diagnosis of AIH (Fig. 3). With regard to the diagnosis of AIH, application of two scoring systems—(1) revised scoring system formulated in 1999 [7] scored 12 points, and (2) simplified criteria for the international AIH guidelines [8] scored 6 points—suggested probable AIH with the present case. The tissue was positive for EBV DNA by PCR qualitative assay (detection limit 2.0×10^1 copies/1.0×10^6 cells equivalent DNA), whereas both the latent membrane protein 1 and EBV-encoded RNA in situ hybridization were negative. Considering the findings of liver biopsy and serological changes, we started steroid administration at 30 mg/day. The dose of steroid was gradually tapered, and the results of serum laboratory tests (alanine aminotransferase [ALT] and IgG levels) improved accordingly. Moreover, the amount of peripheral blood EBV DNA levels, the titers of EBV-VCA IgG and Epstein–Barr nuclear antigen (EBNA) decreased. After steroid administration for 6 months, the patient has remained free of signs and symptoms (Fig. 4).

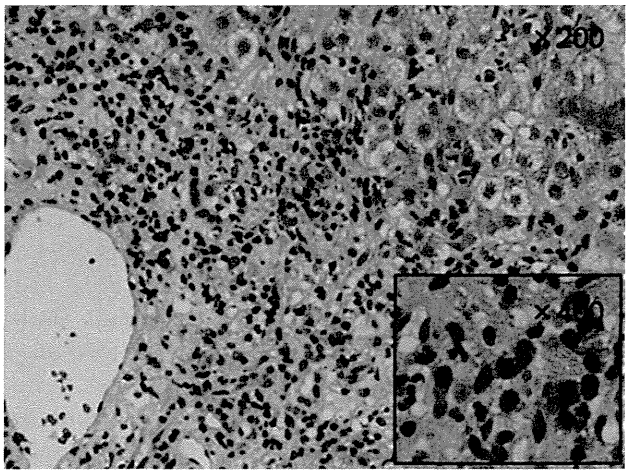

Fig. 3 A second liver biopsy at our hospital before steroid therapy demonstrated fibrotic periportal enlargement, interface hepatitis, and plasma cell infiltration. EBV DNA was positive in the tissue by qualitative PCR assay. ×200 (*lower panel* ×400)

Discussion

The present case had been initially diagnosed as CAEBV. However, the persistent liver enzyme abnormalities prompted us to perform further examinations. Elevation of the ANA titer from 80× (at the initial community hospital) to 320× (at our hospital), along with the pathological changes seen in both of the liver biopsy samples, suggested a diagnosis of AIH, probably resulting from EBV infection.

The pathogenesis of AIH is still unknown, although genetic factors, drug-induced autoimmunity, viral infections, and environmental factors have been thought to trigger AIH [9, 10]. Among these triggering factors, hepatitis A viral infection has been reported [11, 12], although EBV infection appears to be rare in this context. Proposed

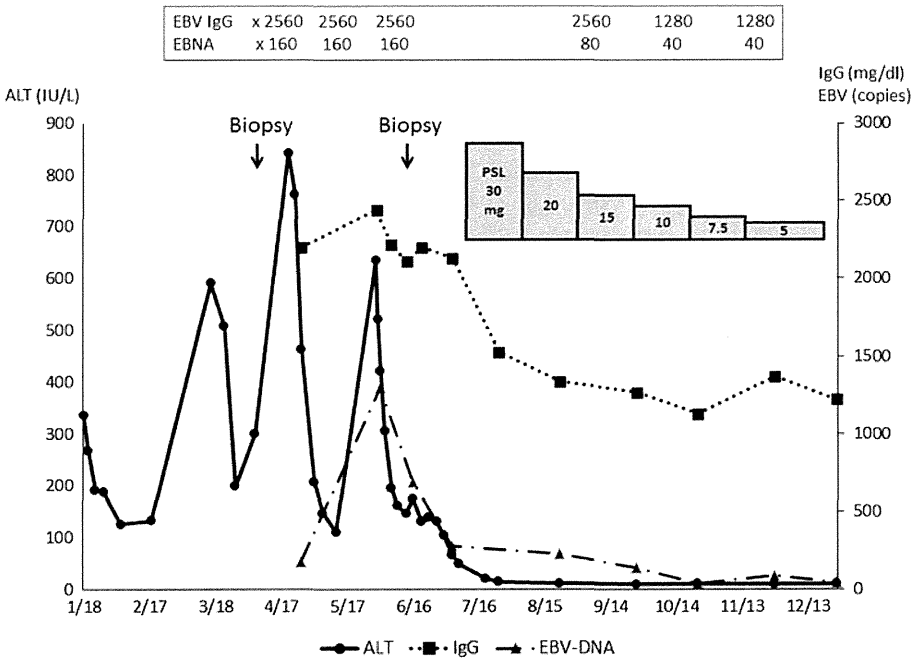

Fig. 4 Clinical course of the present case. Levels of liver enzymes and serum IgG, EBV viral load, EBV IgG, EBNA were ameliorated after steroid administration

mechanisms responsible for inducing autoimmune reactions have included the molecular mimic theory, involving possible similarities between virus-derived exogenous amino acid sequences and host autoantigens [13], although the precise details remain unclear.

On the other hand, the diagnostic criteria for CAEBV formulated by the EBV infection study group in 2003 include (1) persistent or relapsing symptoms of infectious mononucleosis, (2) abnormal antibody reactions to EBV, associated with an elevated titer of VCA or early antigen (EA) antibody, or an increased EBV viral load in the affected organ (including peripheral blood), and (3) a chronic disease course distinct from other known diseases [14]. In the present case, we confirmed that persistent liver enzyme abnormalities were present for >3 months, together with an increased EBV viral load in blood and positive EBV-DNA in hepatic tissue. Compared to the reported case [5], our case seems to be atypical since our case lacked traditional high fever, lymphadenopathy, and allergy to insect bite for CAEBV. However, our patient was older (61 years) than the previous case (14 years) [5], and this may be related to the reason why typical symptoms were missing in the current case. Our patient was treated with prednisolone, and this led to amelioration of the serum ALT and IgG levels, and a decline of the EBV viral load. Antiviral drugs, cytokine therapy, immunosuppressive therapy, cellular transplantation, and allogeneic bone marrow transplantation therapy are reportedly effective for CAEBV, although none of them are established forms of treatment [14]. In our case, immunosuppressive therapy using steroids seems to have been effective so far, and there has been no disease flare-up for 2 years.

In conclusion, we have reported a case of AIH possibly resulting from EBV infection. A possible diagnosis of AIH should be considered in patients with prolonged liver dysfunction subsequent to EBV infection.

Disclosures

Conflict of Interest: Yoshiko Wada, Chikako Sato, Kyoko Tomita, Rika Ishii-Aso, Hiroaki Haga, Kazuo Okumoto, Yuko Nishise, Hisayoshi Watanabe, Tadasih Togashi, Yoshiyuki Ueno declare that they have no conflict of interest.

Human/Animal Rights: All procedures followed were in accordance with the ethical standards of the responsible committee on human experimentation (institutional and national) and with the Helsinki Declaration of 1975, as revised in 2008(5).

Informed Consent: Informed consent was obtained from all patients for being included in the study.

References

1. Rickinson AB. Chronic, symptomatic Epstein–Barr virus-infections. Immunol Today. 1986;7:13–4.
2. Ohshima K, Suzumiya J, Sugihara M, et al. Clinicopathological study of severe chronic active Epstein–Barr virus infection that developed in association with lymphoproliferative disorder and/or hemophagocytic syndrome. Pathol Int. 1998;48:934–43.
3. Okano M, Matsumoto S, Osato T, et al. Severe chronic active Epstein–Barr-virus infection syndrome. Clin Microbiol Rev. 1991;4:129–35.
4. Kimura H, Morishima T, Kanegane H, et al. Prognostic factors for chronic active Epstein–Barr virus infection. J Infect Dis. 2003;187:527–33.
5. Kimura H, Hoshino Y, Kanegane H, et al. Clinical and virologic characteristics of chronic active Epstein–Barr virus infection. Blood. 2001;98:280–6.
6. Kimura H, Morita M, Yabuta Y, et al. Quantitative analysis of Epstein–Barr virus load by using a real-time PCR assay. J Clin Microbiol. 1999;37:132–6.
7. Alvarez E, Berg PA, Bianchi FB, et al. International autoimmune hepatitis group report: review of criteria for diagnosis of autoimmune hepatitis. J Hepatol. 1999;31:929–38.
8. Hennes EM, Zeniya M, Czaja AJ, et al. Simplified criteria for the diagnosis of autoimmune hepatitis. Hepatology. 2008;48:169–76.
9. Krawitt EL. Medical progress: autoimmune hepatitis. N Engl J Med. 2006;354:54–66.
10. Vento S, Guella L, Mirandola F, et al. Epstein–Barr-virus as a trigger for autoimmune hepatitis in susceptible individuals. Lancet. 1995;346:608–9.
11. Vento S, Garofano T, Diperri G, et al. Identification of hepatitis-a virus as a trigger for autoimmune chronic hepatitis type-1 in susceptible individuals. Lancet. 1991;337:1183–7.
12. Huppertz HI, Treichel U, Gassel AM, et al. Autoimmune hepatitis following hepatitis-a virus-infection. J Hepatol. 1995;23:204–8.
13. Wucherpfennig KW. Mechanisms for the induction of autoimmunity by infectious agents. J Clin Invest. 2001;108:1097–104.
14. Okano M, Kawa K, Kimura H, et al. Proposed guidelines for diagnosing chronic active Epstein–Barr virus infection. Am J Hematol. 2005;80:64–9.

THE JOURNAL OF BIOLOGICAL CHEMISTRY VOL. 288, NO. 30, pp. 21861–21875, July 26, 2013

Lack of Oncostatin M Receptor β Leads to Adipose Tissue Inflammation and Insulin Resistance by Switching Macrophage Phenotype*

Received for publication, February 14, 2013, and in revised form, June 7, 2013 Published, JBC Papers in Press, June 11, 2013, DOI 10.1074/jbc.M113.461905

Tadasuke Komori[‡], **Minoru Tanaka**[§], **Emiko Senba**[‡], **Atsushi Miyajima**[§], **and Yoshihiro Morikawa**[‡1]

From the [‡]*Department of Anatomy and Neurobiology, Wakayama Medical University, Wakayama 641-8509, Japan and the* [§]*Laboratory of Cell Growth and Differentiation, Institute of Molecular and Cellular Biosciences, The University of Tokyo, Tokyo 113-0032, Japan*

Background: OSM, a member of IL-6 family of cytokines, is involved in many inflammatory diseases.
Results: OSMRβ$^{-/-}$ mice exhibited phenotypic changes in ATMs to M1, increased proinflammatory cytokines in the adipose tissue, and systemic insulin resistance.
Conclusion: OSMRβ$^{-/-}$ mice exhibited adipose tissue inflammation and insulin resistance preceding obesity.
Significance: OSMRβ$^{-/-}$ mice constitute a unique mouse model of metabolic disorders.

Oncostatin M (OSM), a member of the IL-6 family of cytokines, plays important roles in a variety of biological functions, including inflammatory responses. However, the roles of OSM in metabolic diseases are unknown. We herein analyzed the metabolic parameters of OSM receptor β subunit-deficient (OSMRβ$^{-/-}$) mice under normal diet conditions. At 32 weeks of age, OSMRβ$^{-/-}$ mice exhibited mature-onset obesity, severer hepatic steatosis, and insulin resistance. Surprisingly, insulin resistance without obesity was observed in OSMRβ$^{-/-}$ mice at 16 weeks of age, suggesting that insulin resistance precedes obesity in OSMRβ$^{-/-}$ mice. Both OSM and OSMRβ were expressed strongly in the adipose tissue and little in some other metabolic organs, including the liver and skeletal muscle. In addition, OSMRβ is mainly expressed in the adipose tissue macrophages (ATMs) but not in adipocytes. In OSMRβ$^{-/-}$ mice, the ATMs were polarized to M1 phenotypes with the augmentation of adipose tissue inflammation. Treatment of OSMRβ$^{-/-}$ mice with an anti-inflammatory agent, sodium salicylate, improved insulin resistance. In addition, the stimulation of a macrophage cell line, RAW264.7, and peritoneal exudate macrophages with OSM resulted in the increased expression of M2 markers, IL-10, arginase-1, and CD206. Furthermore, treatment of C57BL/6J mice with OSM increased insulin sensitivity and polarized the phenotypes of ATMs to M2. Thus, OSM suppresses the development of insulin resistance at least in part through the polarization of the macrophage phenotypes to M2, and OSMRβ$^{-/-}$ mice provide a unique mouse model of metabolic diseases.

Obesity is a major factor underlying the development of insulin resistance, which is associated with a number of metabolic disorders, including type 2 diabetes, hypertension, and hyperlipidemia (1). Several lines of evidence now converge on the notion that obesity causes low-grade chronic inflammation characterized by the recruitment of macrophages, T-cells, and neutrophils into the adipose tissue (2–5). Among such inflammatory cells, the increase in adipose tissue macrophages (ATMs)[2] is associated with a further deterioration of adipose tissue inflammation and insulin sensitivity (6, 7). In contrast, a decrease in ATMs in obese mice correlates with the amelioration of adipose tissue inflammation and insulin resistance (8, 9). Therefore, ATMs play important roles in the development of the adipose tissue inflammation and insulin resistance associated with obesity.

Macrophages are a heterogeneous cell population and change their physiology in response to various microenvironmental signals. "Classically activated (M1)" macrophages are induced by two signals, IFN-γ and LPS or TNF (10). On the other hand, "alternatively activated (M2)" macrophages are induced by anti-inflammatory cytokines, such as IL-4 and IL-13 (11). In addition, M1 macrophages produce high levels of toxic intermediates (*e.g.* nitric oxide and reactive oxygen intermediates) via the activation of inducible nitric oxide synthase (iNOS) (12), whereas arginase production is increased in M2 macrophages (13).

It has recently been suggested that a high fat diet triggers the recruitment of M1 macrophages into the adipose tissue, whereas adipose tissue macrophages in lean animals exhibit an M2 phenotype (14). In obese mice, TNF-α, a potent proinflammatory cytokine, is produced by M1 ATMs (7, 15) and directly induces insulin resistance by inhibiting the insulin signaling and insulin-stimulated glucose transport, mainly in the skeletal muscle and white adipose tissue (16, 17). In contrast, M2 ATMs

* This work was supported in part by a Research Grant on Priority Areas from Wakayama Medical University and the 2012 Wakayama Medical Award for Young Researchers.

[1] To whom correspondence should be addressed: Dept. of Anatomy and Neurobiology, Wakayama Medical University, 811-1 Kimiidera, Wakayama 641-8509, Japan. Tel. and Fax: 81-73-441-0617; E-mail: yoshim@wakayama-med.ac.jp.

[2] The abbreviations used are: ATM, adipose tissue macrophage; ANOVA, analysis of variance; CREB, cAMP response element-binding protein; iNOS, nitric oxide synthase; ipGTT, intraperitoneal glucose tolerance test; ITT, insulin tolerance test; MCP, monocyte chemoattractant protein; MGL, macrophage galactose-type C-type lectin; OSM, oncostatin M; OSMRβ, OSM-specific β subunit; OSMRβ$^{-/-}$, OSMRβ-deficient; PE, phycoerythrin; PEM, peritoneal exudate macrophage; RT, room temperature; SVF, stromal vascular fraction.

secrete an anti-inflammatory cytokine, IL-10 (15). The administration of IL-10 in diet-induced obese mice enhances the activation of insulin signaling and insulin-stimulated glucose uptake in the skeletal muscle (18). Thus, the balance between M1/M2 ATMs is important for maintaining the proper balance of pro-/anti-inflammatory cytokine production in the adipose tissue, and its imbalance can lead to the development of insulin resistance. However, the mechanisms underlying the determination of the ATM phenotypes are not fully understood.

Oncostatin M (OSM), a member of the IL-6 family of cytokines, exhibits a variety of biological effects depending on the target cells by binding to a heterodimeric membrane receptor comprising the OSM-specific β subunit (OSMRβ) and gp130 (19). OSM is synthesized by various inflammatory cells, such as activated T-cells, neutrophils, eosinophils, and macrophages (20, 21). In addition, the expression of OSMRβ is induced in human peripheral blood monocytes treated with LPS (22), suggesting that OSM plays an important role in monocyte/macrophage lineage cells during inflammation. However, the roles of OSM in ATMs and in metabolic disorders remain to be elucidated. In the present study we have addressed this question using OSMRβ-deficient ($OSMR\beta^{-/-}$) mice.

EXPERIMENTAL PROCEDURES

Animals—Male C57BL/6J mice (8 weeks old) were purchased from Nihon SLC (Hamamatsu, Japan). The generation of $OSMR\beta^{-/-}$ mice has been described previously (23). $OSMR\beta^{+/+}$ wild-type (WT) and $OSMR\beta^{-/-}$ littermates were obtained from our breeding colony using heterozygous (+/−) breeding pairs. Male and female WT and $OSMR\beta^{-/-}$ mice from 8 to 32 weeks old were used in the present study. All mice were housed in specific pathogen-free facilities and under light (12 h light/dark cycle)-, temperature (22–25 °C)-, and humidity (50–60% relative humidity)-controlled conditions. Mice were allowed free access to food (MF; Oriental Yeast, Tokyo, Japan) and water.

Injection of OSM in C57BL/6J Mice—C57BL/6J mice were injected intraperitoneally with either vehicle or recombinant mouse OSM (12.5 ng/g body weight; R & D Systems, Minneapolis, MN) twice a day (10:00 and 18:00 h) for 1 week.

Injection of Sodium Salicylate in $OSMR\beta^{-/-}$ Mice—$OSMR\beta^{-/-}$ mice were injected intraperitoneally with either vehicle or sodium salicylate (120 μg/g body weight; Sigma) once a day (18:00 h) for 2 weeks.

Isolation of the Adipocyte Fraction and the Stromal Vascular Fraction (SVF)—The mice were deeply anesthetized with diethyl ether, and the epididymal adipose tissue were quickly removed. The adipose tissue was minced into fine pieces and digested with collagenase type 2 (Sigma) with PBS supplemented with 2% FCS at 37 °C for 20 min with high speed shaking. Next, the samples were passed through a 100-μm mesh (BD Biosciences) and fractioned by brief centrifugation (1200 rpm) at room temperature (RT) for 5 min. The floating cells were collected as the adipocyte fraction, and the pellets were collected as the SVF. The cells in the SVF were incubated with ammonium chloride buffer (PharmLyse; BD Biosciences) to lyse the erythrocytes.

Insulin Signaling Analysis—To evaluate insulin signaling, mice fasted for 24 h were intraperitoneally injected with human insulin (10 milliunits/g body weight). Ten minutes later epididymal fat, gastrocnemius muscle, and liver tissue were excised and frozen in liquid nitrogen. Tissue lysates were prepared as described below.

Preparation of Peritoneal Exudate Macrophages (PEMs)—The preparation of PEMs was performed as described previously with some modifications (24). Macrophages elicited in the 3 days after an intraperitoneal injection of 3 ml of thioglycollate medium (BD Biosciences) were harvested by flushing of the peritoneal cavity with Hanks' balanced salt solution (Invitrogen) with plastic syringes, suspended in DMEM (Invitrogen) with 10% FCS, and incubated on 35-mm plastic dishes for 2 h at a density of 1×10^6 cells/dish. Non-adherent cells were discarded, and the adherent cells were cultured at 37 °C for 3 days.

Treatment of PEMs with OSM—PEMs were starved in DMEM with 0.75% bovine serum albumin for 16 h before the stimulation. Then PEMs were treated with PBS or 100 ng/ml concentrations of recombinant mouse OSM and maintained for the appropriate periods.

Cell Culture—Cell culture was performed with some modifications as described previously (25). The mouse macrophage cell line, RAW 264.7, was grown in DMEM (Invitrogen) with 10% FCS, 100 units/ml of penicillin (Invitrogen), and 100 μg/ml of streptomycin (Invitrogen). All cells were grown at 37 °C in a humidified atmosphere of 5% CO_2.

Treatment of LPS and OSM for RAW 264.7 Macrophages—RAW 264.7 macrophages were plated in 35-mm dishes at a density of 1×10^6 cells/dish and cultured in a standard medium for 24 h. The cells were then treated with 10 ng/ml lipopolysaccharide (Sigma) for 16 h and washed by a standard medium twice. Then the cells were treated with vehicle or 100 ng/ml recombinant mouse OSM and maintained for 24 h.

Flow Cytometry—The cells in the SVF were incubated with anti-CD16/CD32 antibodies (1:100, BD Biosciences) to block Fc binding at 4 °C for 20 min followed by incubation with fluorescently labeled primary antibodies or control IgG at 4 °C for 30 min. The FITC-conjugated anti-F4/80, FITC-conjugated rat IgG2a isotype controls, phycoerythrin (PE)-conjugated anti-CD11c, PE-conjugated Armenian hamster IgG2a isotype controls, FITC-conjugated anti-Gr-1, FITC-conjugated rat IgG2b isotype controls, PE-conjugated anti-CD11b, and PE-conjugated rat IgG2b isotype controls were purchased from eBiosciences (San Diego, CA). The PE- or Alexa Fluor 647-conjugated anti-CD206 and their isotype controls were purchased from AbD Serotec (Oxford, UK). To detect OSMRβ in the SVF and PEMs, cells were incubated with goat anti-OSMRβ antibodies (diluted at 1: 5, R&D Systems) or control goat IgG (Jackson ImmunoResearch, West Grove, PA) at 4 °C for 30 min. Then the cells were incubated with PE-conjugated donkey anti-goat IgG (diluted at 1: 20, R&D Systems). The stained cells were analyzed using the C6 flow cytometer (BD Biosciences) or the FACSCalibur flow cytometer (BD Biosciences). Dead cells were removed from the analysis using propidium iodide staining. The flow cytometry results were analyzed using the CFlow (BD Biosciences), the CellQuest software program (BD Biosciences), or FlowJo software suites (Tree Star, Ashland, OR). The

events were first gated based on forward scatter *versus* propidium iodide to identify individual live cells. The plot of a forward *versus* side scatter was used as the second gate to gate out aggregates and debris. Next, the F4/80-positive cells were selected. Single color controls were used to set the compensation and gates.

Western Blot Analysis—Western blot analysis was performed with some modifications as described previously (25). Lysates were prepared by using radioimmune precipitation assay buffer (Upstate Biotechnology, Lake Placid, NY) containing protease inhibitor mixture (Upstate Biotechnology), 1 mM orthovanadate, 1 mM sodium fluoride, and 1 mM phenylmethylsulfonyl fluoride. The protein concentrations in the lysates were determined by using a BCA Protein Assay kit (Pierce). Twenty micrograms of protein from the samples were separated by SDS-PAGE and transferred to PVDF membranes (GE Healthcare). The blotted membranes were incubated with rat anti-CD206 antibody (diluted at 1:500, AbD Serotec), rabbit anti-CD163 antibody (diluted at 1:500, Santa Cruz Biotechnology, Santa Cruz, CA), rabbit anti-iNOS antibody (diluted at 1:500, Abcam, Cambridge, UK), mouse anti-arginase-1 antibody (BD Biosciences), rabbit anti-phosphorylated Akt antibody (diluted at 1:1000, Cell Signaling Technology, Beverly, MA), rabbit anti-Akt antibody (diluted at 1:1000, Cell Signaling Technology), rabbit anti-phosphorylated STAT3 antibody (diluted at 1:1000, Cell Signaling Technology), rabbit anti-STAT3 antibody (diluted at 1:1000, Cell Signaling Technology), rabbit anti-phosphorylated cAMP response element-binding protein (CREB) antibody (diluted at 1:1000, Cell Signaling Technology), and rabbit anti-CREB antibody (diluted at 1:1000, Cell Signaling Technology). Then the membranes were incubated with HRP-conjugated donkey anti-goat (diluted at 1:4,000, GE Healthcare), donkey anti-rat (diluted at 1:10,000, Jackson ImmunoResearch), donkey anti-rabbit (diluted at 1:20,000, GE Healthcare), or donkey anti-mouse (diluted at 1:20,000, GE Healthcare) IgG antibodies. Labeled proteins were detected with chemiluminescence using ECL detection reagent (GE Healthcare) according to the manufacturer's instructions. The membranes were exposed to hyperfilm ECL (GE Healthcare) for an appropriate period. The blotted membranes were stripped in 0.25 M glycine, pH 2.5, at RT for 10 min and incubated with rat anti-tubulin antibody (diluted at 1:500; Abcam) at 4 °C for 16 h followed by the incubation with HRP-conjugated donkey anti-rat antibody (diluted at 1:4000) at RT for 1 h.

Immunohistochemistry—Immunofluorescence staining was performed with some modifications as described previously (26, 27). Briefly, mice were deeply anesthetized with diethyl ether, and the epididymal fat pads were quickly removed. Then the fat pads were fixed with 1% paraformaldehyde in PBS at 4 °C for 1 h followed by the preincubation in 5% normal donkey serum at RT for 1 h. Then the fat pads were incubated with goat anti-OSM antibody (diluted at 1:400), goat anti-OSMRβ antibody (diluted at 1:400), rat anti-F4/80 antibody (diluted at 1:1000; AbD Serotec), and rabbit anti-caveolin-1 antibody (diluted at 1:400; BD Biosciences). The fat pads were incubated with Cy2-conjugated, Cy3-conjugated, or biotinylated secondary antibodies (diluted at 1:800; Jackson ImmunoResearch) at RT for 1 h. Then the fat pads were incubated with 7-amino-4-methylcoumarin-3-acetic acid-conjugated streptavidin (diluted at 1:500; Jackson ImmunoResearch) at RT for 30 min and mounted in the mounting media (90% glycerol and 10% PBS) on the chambered slide. Immunofluorescence images were acquired using a confocal laser scanning microscope (LSM700; Carl Zeiss, Tokyo, Japan).

To complete an immunohistochemical analysis in pancreas, mice were deeply anesthetized with diethyl ether and transcardially perfused with ice-cold 0.85% NaCl followed by ice-cold Zamboni's fixative (2% paraformaldehyde and 0.2% picric acid in 0.1 M PBS). Tissues were quickly removed, postfixed in the same fixative at 4 °C for 3 h, and cryoprotected in 20% sucrose in 0.1 M PBS. All specimens were frozen rapidly in cold *n*-hexane on dry ice and stored at −80 °C. Frozen sections were cut on a cryostat (6-μm thickness). The sections were preincubated in 5% normal donkey serum at RT for 1 h followed by the incubation with rabbit anti-insulin antibody (diluted at 1:400; Abcam). Then they were incubated with biotinylated donkey anti-rabbit IgG antibody (diluted at 1:800; Jackson ImmunoResearch) at RT for 1 h followed by incubation with HRP-conjugated streptavidin (DAKO, Carpinteria, CA) at RT for 30 min. Thereafter, the peroxidase reaction product was visualized with 0.05% diaminobenzidine tetrahydrochloride (Sigma) and 0.01% H_2O_2. After the reaction, the sections were counterstained with Eosin Y (Muto Pure Chemical, Tokyo, Japan). Images were acquired by using a BIOREVO BZ-9000 microscope (KEYENCE, Osaka, Japan). To evaluate the area of β-cell in pancreas, every 20th section was selected from a series of consecutive pancreatic sections (6 μm), and 12 sections per mouse were used for analysis. For each section the cells were considered to be positive for insulin if the cell bodies were stained brown. The area of β-cells and pancreas was measured by using Image J analysis software (Version 1.46r, Scion, Frederick, MD).

The following controls were performed: (i) incubation with protein A-purified goat or rabbit IgG instead of primary antibody; (ii) incubation without the primary antibody or without primary and secondary antibodies. None of the controls revealed any labeling (data not shown).

Measurement of Blood Glucose and Serum Insulin—These procedures were performed with some modifications as described previously (28). Mice were fasted for 4 h to remove the effects of food intake on glucose metabolism, and blood was taken from the tail vein at 18:00 h. In fasting experiments, mice were fasted for 24 h with free access to water. Then serum was immediately collected and stored at −20 °C. Blood glucose levels were measured by a glucose measurement device (Glucocard GT-1640, Arkray, Kyoto, Japan). The serum insulin concentrations were determined using kits from Morinaga (Tokyo, Japan).

Intraperitoneal Glucose Tolerance Test (ipGTT) and Insulin Tolerance Test (ITT)—For ipGTT, the mice were fasted for 16 h and received an intraperitoneal injection of D-glucose (1 g/kg body weight). The blood samples were collected from the tail vein before and at 15, 30, 60, and 120 min after the injection of D-glucose. For ITT, mice were fasted for 4 h and received an intraperitoneal injection of insulin (1 unit/kg body weight). The

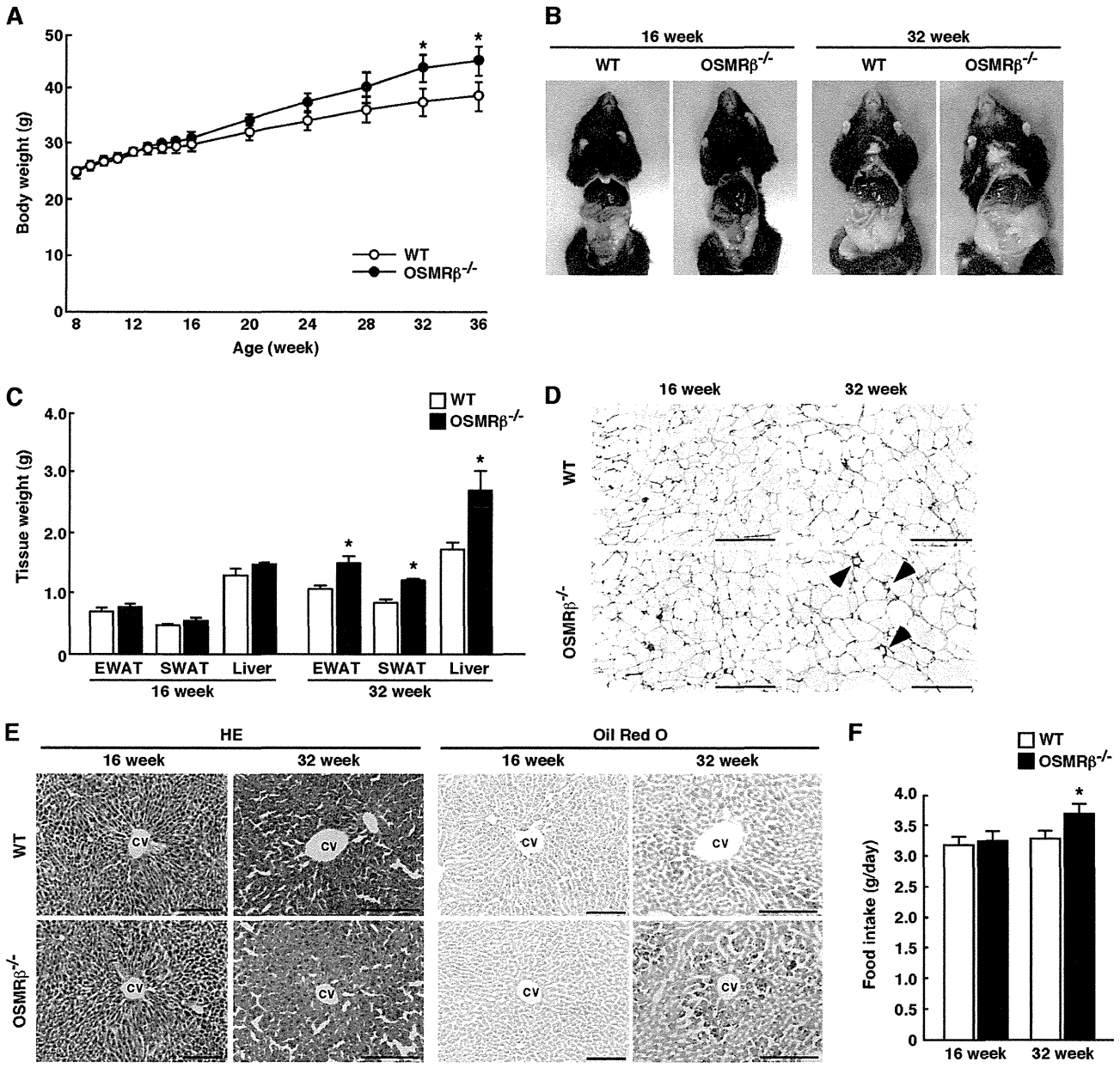

FIGURE 1. **The characteristics of WT and OSMRβ$^{-/-}$ mice under normal diet conditions.** *A*, shown are the body weights of WT and OSMRβ$^{-/-}$ mice from 8 to 36 weeks of age ($n = 6–10$). *B*, shown are representative images of WT and OSMRβ$^{-/-}$ mice at 16 and 32 weeks of age. *C*, shown are the tissue weights in WT and OSMRβ$^{-/-}$ mice at 16 and 32 weeks of age ($n = 6–10$). *EWAT*, epididymal white adipose tissue; *SWAT*, subcutaneous white adipose tissue. *D*, shown is a histological analysis with H&E (*HE*) staining in the EWAT in WT and OSMRβ$^{-/-}$ mice at 16 and 32 weeks of age. *Arrowheads* indicate crown-like structures. *Scale bars* = 200 μm. *E*, shown is a histological analysis with H&E staining and Oil Red O staining in the liver of WT and OSMRβ$^{-/-}$ mice at 16 and 32 weeks of age. *CV*, central vein. *Scale bars* = 100 μm. *F*, food intake in WT and OSMRβ$^{-/-}$ mice at 16 and 32 weeks of age ($n = 6–10$) is shown. The data represent the mean ± S.E. *, $p < 0.05$ WT *versus* OSMRβ$^{-/-}$ mice, ANOVA followed by the post-hoc Bonferroni test (A); Student's *t* test (*C* and *F*).

blood samples were collected from the tail vein before and at 15, 30, 60, and 120 min after the injection of insulin.

ELISA—Concentrations of serum TNF-α, IL-6, IL-10, adiponectin, and monocyte chemoattractant protein-1 (MCP-1) were measured by ELISA kits (R & D Systems) according to the manufacturer's instructions. The serum concentrations of leptin, serum amyloid A, and OSM were determined using ELISA kits from Morinaga, Invitrogen, and USCN Life Science (Wuhan, China), respectively.

Measurement of Lipid Content in the Serum and Liver—The serum levels of triglycerides, total cholesterol, and free fatty acids were measured at Nagahama Life Science Laboratory (Nagahama, Japan) using lipid assay kits (Triglyceride E-Test Wako, Total Cholesterol E-Test Wako, and NEFA C-Test Wako, Wako Pure Chemical Industries, Osaka, Japan) according to the manufacturer's instructions.

The contents of the triglycerides and total cholesterol in the liver were analyzed at Skylight Biotech (Akita, Japan). Lipids were extracted from the livers using the Folch method (29). Frozen liver tissues were homogenized, and triglycerides and total cholesterol were extracted from the homogenate with chloroform/methanol (2:1, v/v), dried, and resus-

TABLE 1

Various metabolic parameters in the serum and liver of WT and OSMR $\beta^{-/-}$ mice at 16 and 32 weeks of age ($n = 6-8$)

The data represent the mean ± S.E.

Parameters (units)	WT (16 weeks)	OSMR$\beta^{-/-}$ (16 weeks)	WT (32 weeks)	OSMR$\beta^{-/-}$ (32 weeks)
Serum concentrations				
Total cholesterol (mg/dl)	94.2 ± 8.1	90.2 ± 3.1	102.7 ± 4.6	141.3 ± 0.7[a]
Triglyceride (mg/dl)	107.0 ± 10.0	102.7 ± 13.1	87.7 ± 8.3	102.0 ± 5.8[a]
Free fatty acid (mmol/liter)	1.40 ± 0.16	1.51 ± 0.07	1.90 ± 0.02	1.98 ± 0.01[a]
Leptin (ng/ml)	5.97 ± 0.39	7.32 ± 1.63	12.6 ± 2.8	18.8 ± 2.5[a]
Serum amyloid A (ng/ml)	8.84 ± 1.74	14.24 ± 1.93[a]	14.9 ± 1.4	30.6 ± 6.4[a]
TNF-α (pg/ml)	3.61 ± 0.24	4.67 ± 0.45[a]	4.22 ± 0.62	5.69 ± 0.85[a]
IL-6 (pg/ml)	0.27 ± 0.05	0.31 ± 0.08	0.51 ± 0.06	0.68 ± 0.06[a]
MCP-1 (pg/ml)	20.1 ± 0.6	24.3 ± 2.1[a]	46.9 ± 7.6	84.2 ± 11.2[a]
IL-10 (pg/ml)	7.04 ± 0.57	5.55 ± 0.43[a]	10.6 ± 0.6	9.08 ± 0.61[a]
Adiponectin (μg/ml)	25.1 ± 2.1	22.2 ± 0.8[a]	15.3 ± 0.7	13.2 ± 0.5[a]
OSM (pg/ml)	64.7 ± 8.1	60.92 ± 7.7	46.9 ± 9.7	73.5 ± 11.8[a]
Glucose (fed) (mg/dl)	135.3 ± 12.7	152.0 ± 9.1	162.0 ± 16.3	198.3 ± 18.1[a]
Insulin (fed) (ng/ml)	0.66 ± 0.05	5.41 ± 1.60[a]	2.10 ± 0.11	9.98 ± 0.60[b]
Glucose (fasted) (mg/dl)	68.7 ± 2.6	64.0 ± 3.1	80.0 ± 4.2	89.7 ± 2.9[a]
Insulin (fasted) (ng/ml)	0.31 ± 0.09	2.21 ± 0.71[a]	0.96 ± 0.33	5.63 ± 0.21[b]
Liver concentrations				
Total cholesterol (mg/g)	2.03 ± 0.10	2.23 ± 0.06	2.10 ± 0.03	3.12 ± 0.20[a]
Triglyceride (mg/g)	9.82 ± 3.21	13.6 ± 2.9	15.2 ± 0.4	105.4 ± 18.4[b]

[a] $p < 0.05$ WT *versus* OSMR$\beta^{-/-}$ mice; Student's *t* test.
[b] $p < 0.01$ WT *versus* OSMR$\beta^{-/-}$ mice; Student's *t* test.

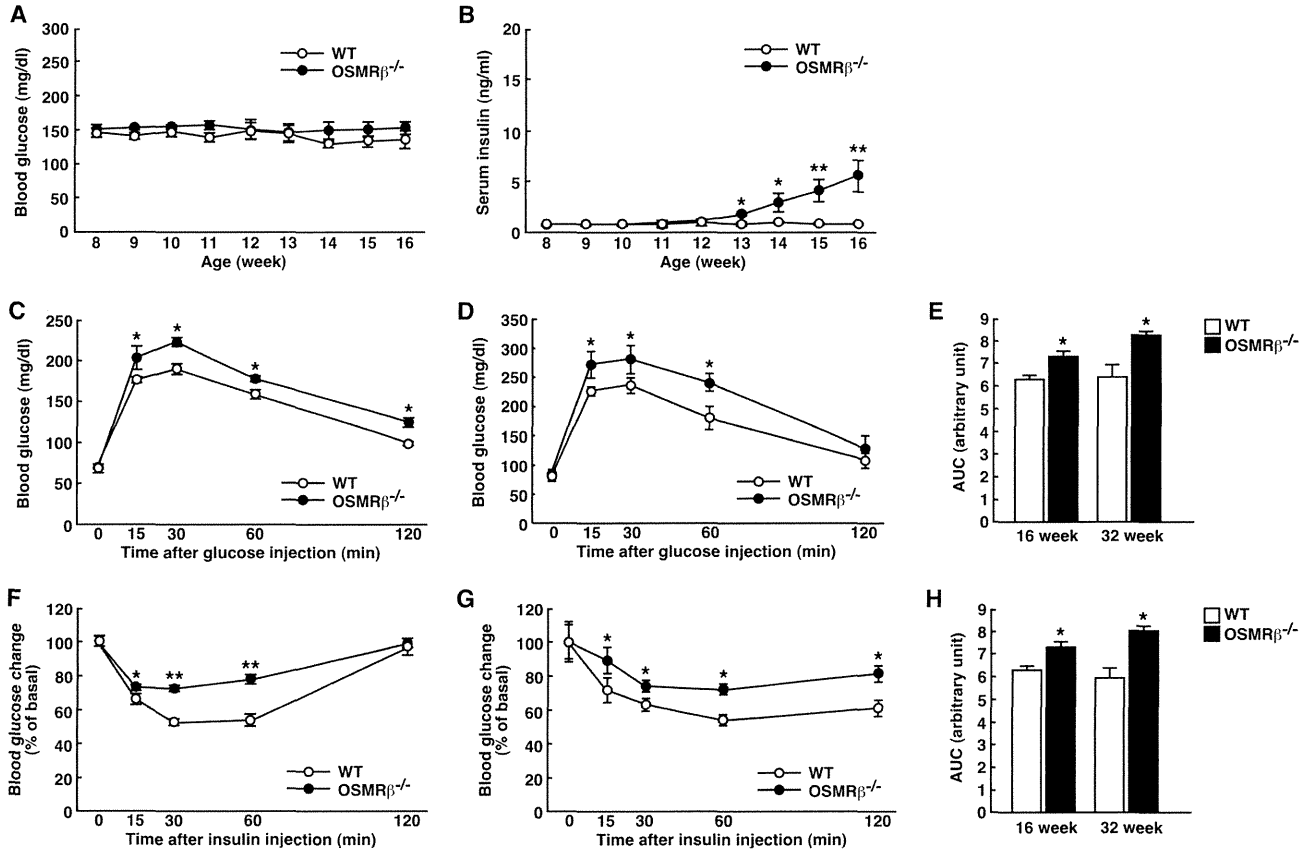

FIGURE 2. **Glucose intolerance and insulin resistance in OSMR$\beta^{-/-}$ mice under normal diet conditions.** *A* and *B*, shown are blood glucose (*A*) and serum insulin (*B*) levels in WT and OSMR$\beta^{-/-}$ mice from 8 to 16 weeks of age ($n = 6$). *C–H*, shown are the results of the ipGTTs (*C* and *D*) and ITTs (*F* and *G*) in WT and OSMR$\beta^{-/-}$ mice at 16 (*C* and *F*) and 32 (*D* and *G*) weeks of age ($n = 6$). The areas under the curves (*AUC*) for blood glucose in the ipGTTs (*E*) and ITTs (*H*) are shown. The data represent the mean ± S.E. *, $p < 0.05$; **, $p < 0.01$ WT *versus* OSMR$\beta^{-/-}$ mice, ANOVA followed by the post-hoc Bonferroni test (*A–D*, *F*, and *G*); Student's *t* test (*E* and *H*).

pended in 2-propanol. The amounts of triglycerides and total cholesterol in the extract were measured using lipid assay kits (Cholestest TG and Cholestest CHO, Sekisui Medical, Tokyo, Japan).

Quantitative Real-time PCR—Quantitative real-time PCR was performed with some modifications as described previously (25). Briefly, total RNAs from PEMs were prepared using TRI reagent (Molecular Research Center, Cincinnati,

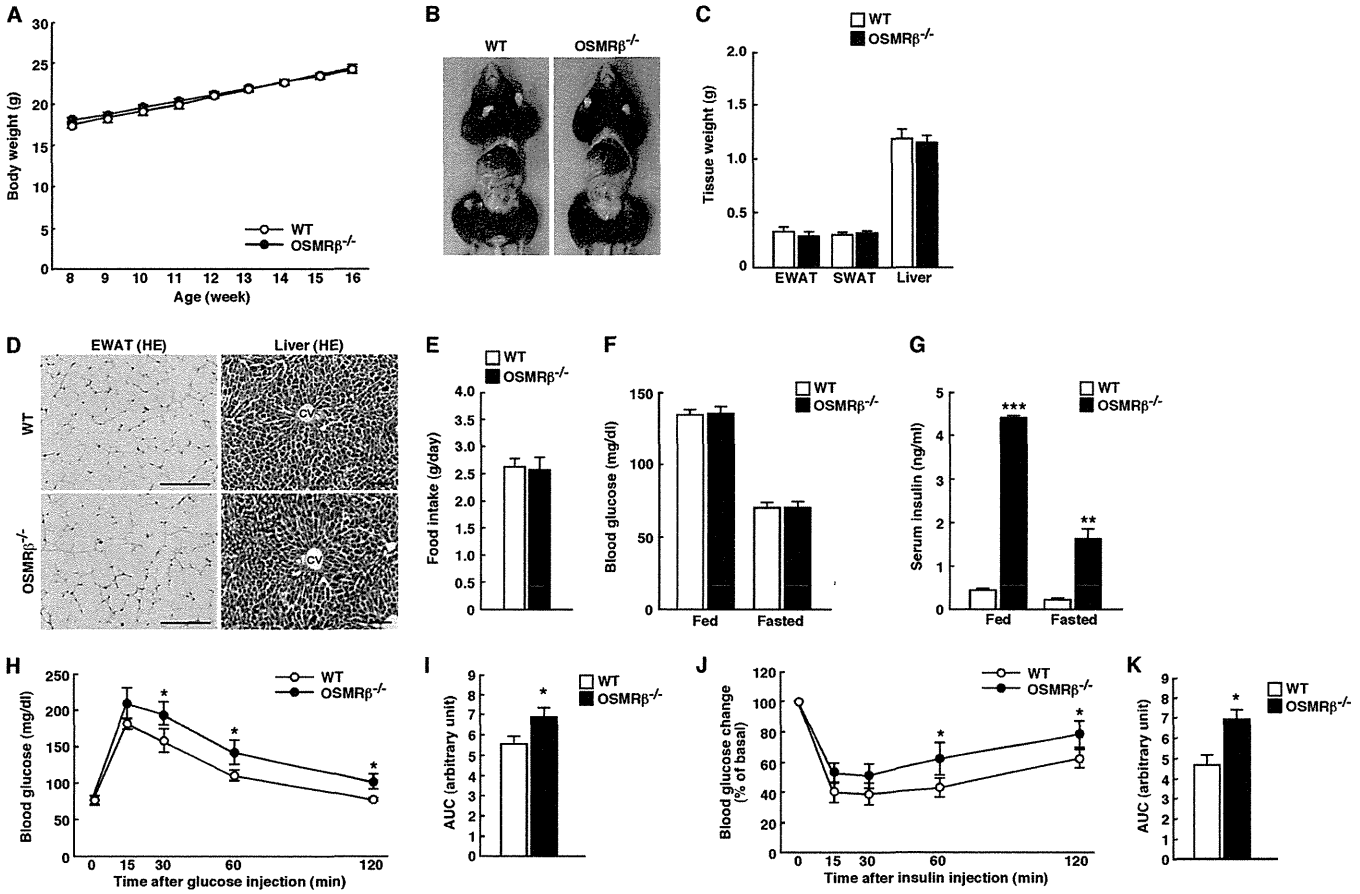

FIGURE 3. **The characteristics of female WT and OSMRβ$^{-/-}$ mice under normal diet conditions.** *A*, shown are the body weights of female WT and OSMRβ$^{-/-}$ mice from 8 to 16 weeks of age ($n = 6$). *B*, shown are representative images of female WT and OSMRβ$^{-/-}$ mice at 16 weeks of age. *C*, shown are the tissue weights in female WT and OSMRβ$^{-/-}$ mice at 16 weeks of age ($n = 6$). *EWAT*, epididymal white adipose tissue; *SWAT*, subcutaneous white adipose tissue. *D*, shown is a histological analysis with H&E (*HE*) staining in the epididymal white adipose tissue and liver in female WT and OSMRβ$^{-/-}$ mice at 16 weeks of age. *CV*, central vein. *Scale bars* = 200 μm (epididymal white adipose tissue); 100 μm (liver). *E*, shown is food intake in female WT and OSMRβ$^{-/-}$ mice at 16 weeks of age ($n = 6$). *F* and *G*, shown are blood glucose (*F*) and serum insulin (*G*) levels in female WT and OSMRβ$^{-/-}$ mice at 16 weeks of age under fed and fasted conditions. *H–K*, shown are the results of the ipGTTs (*H*) and ITTs (*J*) in female WT and OSMRβ$^{-/-}$ mice at 16 weeks of age ($n = 6$). The areas under the curves (*AUC*) for blood glucose in the ipGTTs (*I*) and ITTs (*K*) are shown. The data represent the mean ± S.E. *, $p < 0.05$; **, $p < 0.01$; ***, $p < 0.005$ WT *versus* OSMRβ$^{-/-}$ mice, ANOVA followed by the post-hoc Bonferroni test (*A*, *H*, and *J*); Student's *t* test (*C*, *E*, *F*, *G*, *I*, and *K*).

OH). The cDNA from the total RNA was synthesized with TaqMan Reverse Transcription Reagents (Applied Biosystems, Foster City, CA). The following TaqMan Gene Expression Assays (Applied Biosystems) were used: TNF-α (Mm00443258_m1), IL-1β (Mm00434228_m1), IFN-γ (Mm00801778_m1), MCP-1 (Mm00441242_m1), C-C chemokine receptor 2 (CCR2) (Mm00438270_m1), toll-like receptor 4 (TLR4) (Mm00445273_m1), IL-6 (Mm00446190_m1), IL-10 (Mm00439616_m1), IL-13 (Mm00434204_m1), adiponectin (Mm00456425_m1), macrophage galactose-type C-type lectin (MGL) 1 (Mm00546124_m1), MGL2 (Mm00460844_m1), OSM (Mm01193966_m1), OSMRβ (Mm00495424_m1), and 18 S (Hs99999901_s1). Quantitative real-time PCR for each gene was performed using Rotor Gene Q (Qiagen, Hilden, Germany) and Rotor Gene Probe PCR kits (Qiagen). The PCR amplification protocol was 95 °C for 10 min and then 40 cycles of 95 °C for 10 s and 60 °C for 45 s. The relative abundance of transcripts was normalized by the expression of 18 S mRNA and analyzed using ΔΔCT method.

Statistical Analysis—The results are shown as the means ± S.E. Statistically significant differences between groups were analyzed by Student's *t* test or an analysis of variance (ANOVA) followed by the post-hoc Bonferroni test. The criterion for statistical significance was $p < 0.05$.

RESULTS

Systemic Changes of Metabolic Parameters in OSMRβ$^{-/-}$ Mice—To assess the roles of OSMRβ in the metabolic diseases, we analyzed OSMRβ$^{-/-}$ mice under normal diet conditions. The macroscopic findings, body weights, and tissue weights (epididymal adipose tissue, subcutaneous adipose tissue, and liver) did not differ significantly between WT and OSMRβ$^{-/-}$ mice until 16 weeks of age (Fig. 1, *A–C*). However, OSMRβ$^{-/-}$ mice began to be heavier than WT mice at 20 weeks of age, and the significant increase in body weights compared with WT mice was observed in OSMRβ$^{-/-}$ mice at 32 weeks of age (Fig. 1*A*). At 32 weeks of age, the weights of the adipose tissue and liver in OSMRβ$^{-/-}$ mice were heavier than those in WT mice (Fig. 1, *B* and *C*). As shown in Fig. 1*D*, in the adipose tissue of OSMRβ$^{-/-}$ mice the adipocytes appeared to be larger than those in WT mice, and crown-like structures were also observed. In addition, lipid accumulation was greater in the

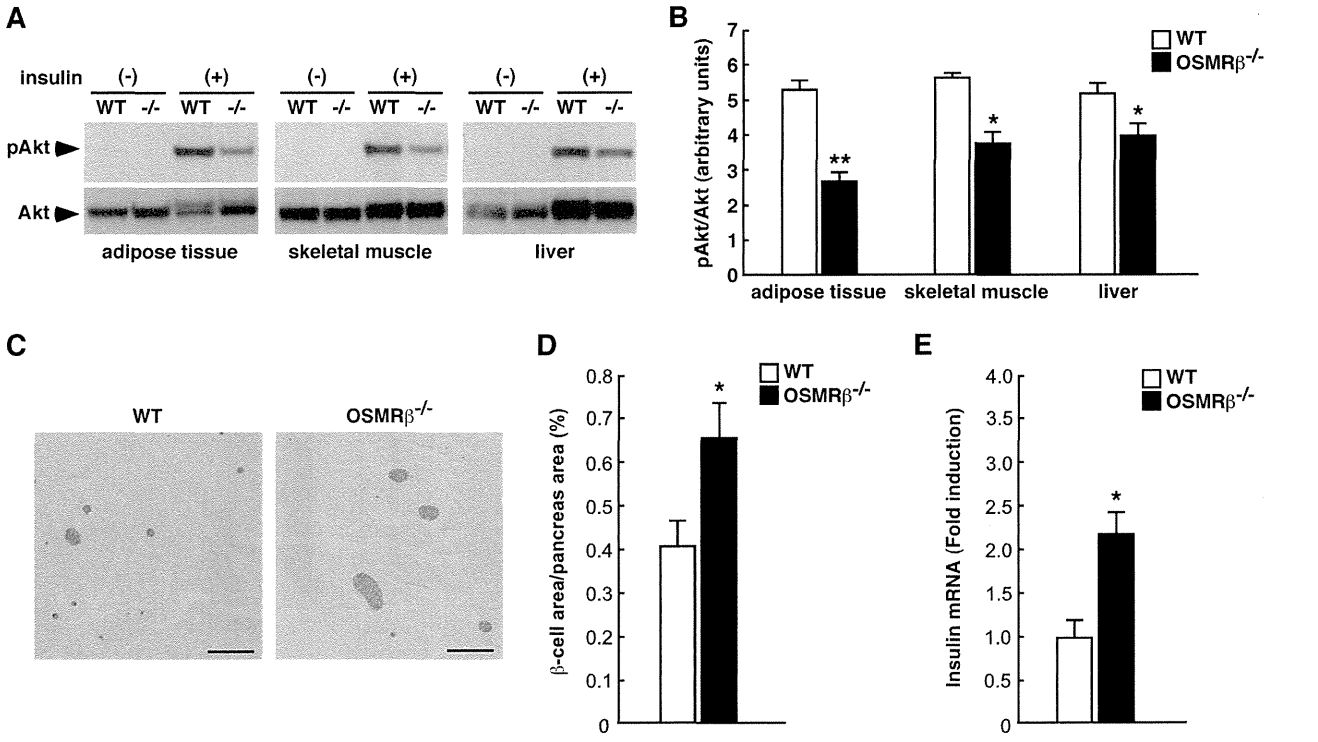

FIGURE 4. **Reduced insulin signaling and pancreatic β-cell hyperplasia in OSMRβ$^{-/-}$ mice at 16 weeks of age under normal diet conditions.** *A*, shown is insulin-stimulated Akt phosphorylation in the adipose tissue, skeletal muscle, and liver of WT and OSMRβ$^{-/-}$ mice. *B*, shown is quantitative analysis of phosphorylation of Akt in the adipose tissue, skeletal muscle, and liver of WT and OSMRβ$^{-/-}$ mice ($n = 6$). *C–E*, shown are hyperplasia of β-cells and insulin production in the pancreas of WT and OSMRβ$^{-/-}$ mice. *C*, shown is immunohistochemistry for insulin (*black*) in the pancreas of WT and OSMRβ$^{-/-}$ mice. Scale bars = 500 μm. *D*, shown is quantitative analysis of the area of β-cells in the total area of the pancreas. *E*, shown is the mRNA expression of insulin in the pancreas of WT and OSMRβ$^{-/-}$ mice. The data represent the mean ± S.E. *, $p < 0.05$; **, $p < 0.01$ WT *versus* OSMRβ$^{-/-}$ mice, Student's *t* test (*B*, *D*, and *E*).

livers of OSMRβ$^{-/-}$ mice compared with that in WT mice at 32 weeks of age (Fig. 1*E*). However, the adipose tissue and liver were histologically normal in OSMRβ$^{-/-}$ mice at 16 weeks of age (Fig. 1, *D* and *E*). Although there was no difference in the amount of food intake between WT and OSMRβ$^{-/-}$ mice at 16 weeks of age, OSMRβ$^{-/-}$ mice showed hyperphagia at 32 weeks of age (Fig. 1*F*).

The serum concentration of leptin in OSMRβ$^{-/-}$ mice was higher than that in WT mice at 32 weeks of age, although it was not changed between WT and OSMRβ$^{-/-}$ mice at 16 weeks of age (Table 1). Both serum lipid levels (total cholesterol, triglyceride, and free fatty acid) and lipid contents in the liver (total cholesterol and triglyceride) were higher in OSMRβ$^{-/-}$ mice at 32 weeks of age (Table 1). Neither the serum lipid levels nor lipid contents in the liver were different between WT and OSMRβ$^{-/-}$ mice at 16 weeks of age (Table 1).

To investigate the systemic inflammation in OSMRβ$^{-/-}$ mice, we analyzed the serum levels of some inflammatory markers. The serum concentrations of serum amyloid A, TNF-α, IL-6, and MCP-1 were higher, whereas the concentrations of IL-10 and adiponectin in the serum were lower in OSMRβ$^{-/-}$ mice than in WT mice at 32 weeks of age (Table 1). The changes in those inflammatory markers, except for IL-6, were already observed at 16 weeks of age (Table 1). Serum concentration of IL-6 also tended to increase but not significantly in OSMRβ$^{-/-}$ mice at 16 weeks of age (Table 1).

At 32 weeks of age, both blood glucose and serum insulin levels in fed and fasted conditions were higher in OSMRβ$^{-/-}$ mice compared with those in WT mice (Table 1). At 16 weeks of age, there were no differences in blood glucose levels between WT and OSMRβ$^{-/-}$ mice, whereas serum insulin levels were higher in OSMRβ$^{-/-}$ mice in both fed and fasted conditions (Table 1).

Similar to the male mice, neither female WT nor female OSMRβ$^{-/-}$ mice showed any differences in body weight, tissue weights, or food intake (see Fig. 3, *A–E*). The blood glucose levels did not differ between WT and OSMRβ$^{-/-}$ mice; however, the serum insulin levels were increased in OSMRβ$^{-/-}$ mice in fed and fasted conditions at 16 weeks of age (see Fig. 3, *F* and *G*). These results suggest that OSMRβ$^{-/-}$ mice exhibit systemic inflammation and disturbance of glucose metabolism preceding obesity. We next analyzed glucose and insulin levels in more detail.

OSMRβ$^{-/-}$ Mice Develop Glucose Intolerance and Insulin Resistance—To examine the effects of OSMRβ deficiency on glucose metabolism, we measured the blood glucose and serum insulin levels once a week for 8 weeks in WT and OSMRβ$^{-/-}$ mice under normal diet conditions. As shown in Fig. 2*A*, there were no significant changes in the blood glucose levels between WT and OSMRβ$^{-/-}$ mice until 16 weeks of age. However, the serum insulin levels began to increase in OSMRβ$^{-/-}$ mice compared with those observed in WT mice starting from 13 weeks of age (Fig. 2*B*). In addition, ipGTTs and ITTs revealed that OSMRβ$^{-/-}$ mice displayed glucose intolerance and insulin resistance at both 16 and 32 weeks of age (Fig. 2, *C–H*). Consistent with the data in the male mice, the female

OSMR$\beta^{-/-}$ mice at 16 weeks of age exhibited glucose intolerance and insulin resistance, as measured with ipGTTs and ITTs (Fig. 3, *H–K*).

To investigate the tissue-specific insulin resistance in OSMR$\beta^{-/-}$ mice at 16 weeks of age, we analyzed insulin-stimulated Akt phosphorylation in the adipose tissue, skeletal

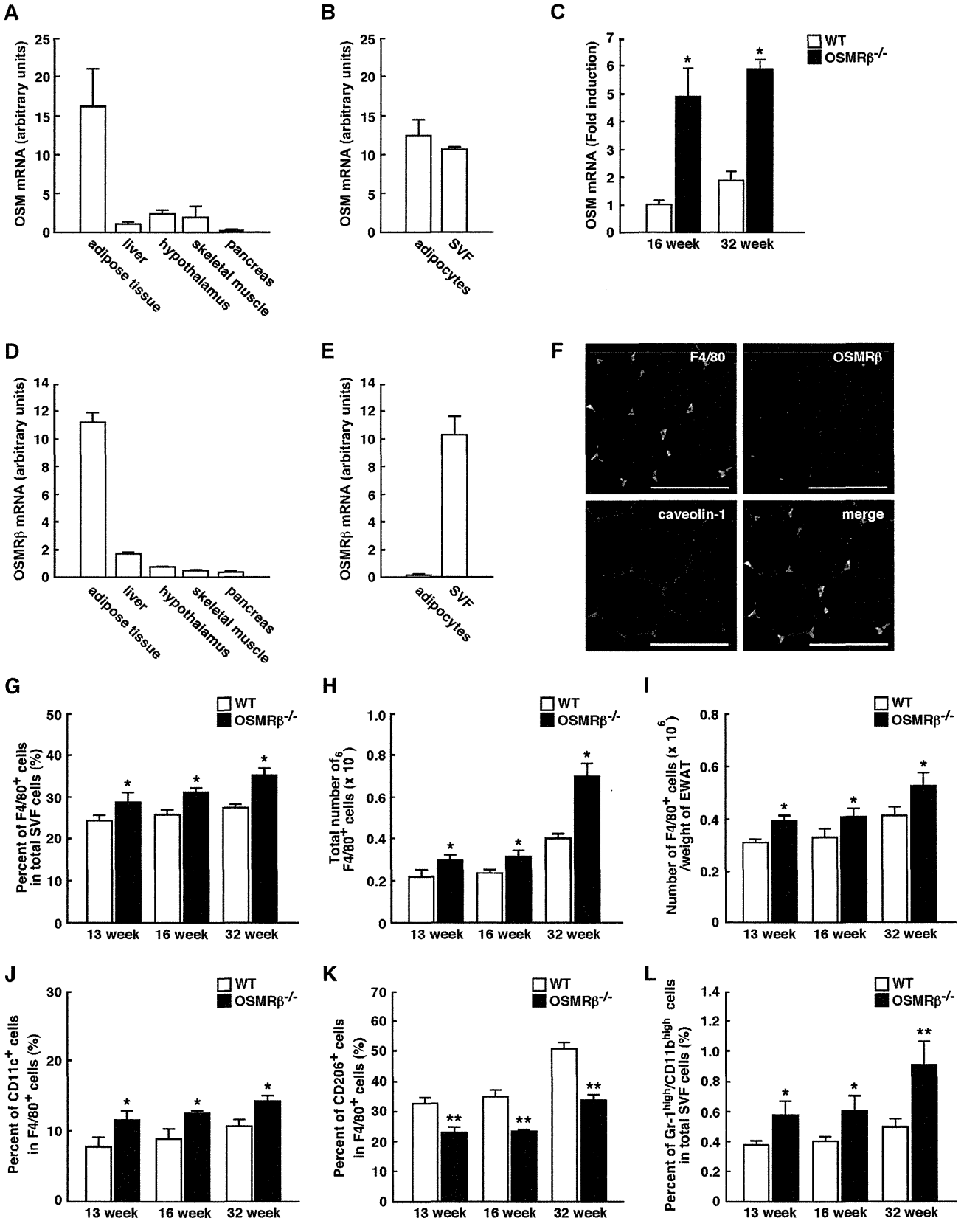

muscle, and liver. Insulin-stimulated Akt phosphorylation was decreased in the adipose tissue, skeletal muscle, and liver in OSMR$\beta^{-/-}$ mice compared with that observed in WT mice (Fig. 4, *A* and *B*). Histological examination of pancreas revealed that the percentages of insulin-positive areas (β-cells) among total areas of the pancreas were higher in OSMR$\beta^{-/-}$ mice compared with those in WT mice at 16 weeks of age (Fig. 4, *C* and *D*), suggesting that OSMR$\beta^{-/-}$ mice exhibit hyperplasia of β-cells in the pancreas. In addition, the expression of insulin mRNA was increased in the pancreas of OSMR$\beta^{-/-}$ mice compared with that in WT mice at 16 weeks of age (Fig. 4*E*).

Adipose Tissue Inflammation and Phenotypes of ATMs in OSMR$\beta^{-/-}$ Mice—It is well established that obesity-induced adipose tissue inflammation is important for the development of insulin resistance (5). Both OSM and OSMRβ were expressed strongly in the adipose tissue and little in the liver, hypothalamus, skeletal muscle, and pancreas at 16 weeks of age (Fig. 5, *A* and *D*). In the adipose tissue, the expression of OSM was observed in both SVF and adipocyte fractions (Fig. 5*B*). In contrast, OSMRβ was mainly expressed in the SVF, whereas the expression of OSMRβ was rarely detected in the adipocyte fraction (Fig. 5*E*).

Serum concentration of OSM was not changed between WT and OSMR$\beta^{-/-}$ mice at 16 weeks of age (Table 1). However, the expression of OSM mRNA in the adipose tissue was increased in OSMR$\beta^{-/-}$ mice compared with that in WT mice (Fig. 5*C*). At 32 weeks of age, both serum concentration of OSM and the expression of OSM mRNA in the adipose tissue were higher in OSMR$\beta^{-/-}$ mice compared with those in WT mice (Fig. 5*C* and Table 1).

In addition, double-immunofluorescence staining revealed that OSMRβ was exclusively expressed in F4/80-positive macrophages in the adipose tissue (Fig. 5*F*). Therefore, OSM appears to act primarily on macrophages in the adipose tissue.

Next we examined the phenotypes of ATMs in OSMR$\beta^{-/-}$ mice under normal diet conditions. The flow cytometric analyses of the SVF showed that the percentages and total numbers of F4/80-positive cells were increased in OSMR$\beta^{-/-}$ mice compared with those observed in WT mice at 13, 16, and 32 weeks of age (Fig. 5, *G–I*). To discriminate between M1 and M2 ATMs with flow cytometry, we used antibodies against CD11c and CD206 as markers of M1 and M2 ATMs, respectively (15). The percentages of CD11c-positive M1 ATMs among the total numbers of ATMs were higher in OSMR$\beta^{-/-}$ mice than in WT mice (Fig. 5*J*). In contrast, the percentages of CD206-positive M2 ATMs among the total numbers of ATMs were lower in OSMR$\beta^{-/-}$ mice than in WT mice (Fig. 5*K*). In addition, the percentages of neutrophils, which highly expressed both Gr-1 and CD11b, among total SVF cells were higher in OSMR$\beta^{-/-}$ mice than in WT mice (Fig. 5*L*). Such changes in the phenotypes of ATMs were also observed at 13 weeks of age when serum insulin levels just started to rise (Fig. 5, *J–L*). These results indicate that OSMR$\beta^{-/-}$ mice exhibit phenotypic changes in ATMs to M1 at 13, 16, and 32 weeks of age.

To evaluate the adipose tissue inflammation in OSMR$\beta^{-/-}$ mice at 16 weeks of age, we examined the expression levels of various pro- and anti-inflammatory markers. The gene expressions of proinflammatory markers, including TNF-α, IL-1β, IFN-γ, MCP-1, CCR2, and TLR4, were more abundant in the adipose tissue and SVF of OSMR$\beta^{-/-}$ mice than in the adipose tissue and SVF of WT mice (Fig. 6, *A* and *B*). In contrast, the gene expressions of anti-inflammatory markers, including IL-10, IL-13, MGL1, and MGL2, in the adipose tissue and SVF of OSMR$\beta^{-/-}$ mice were lower than those observed in the adipose tissue and SVF of WT mice (Fig. 6, *A* and *B*). The gene expression of adiponectin in the adipose tissue also decreased in OSMR$\beta^{-/-}$ mice (Fig. 6*A*). There were no differences in the IL-6 gene expression levels in the adipose tissue and SVF between WT and OSMR$\beta^{-/-}$ mice (Fig. 6, *A* and *B*). Although iNOS was expressed more abundantly in the adipose tissue of OSMR$\beta^{-/-}$ mice than in the adipose tissue of WT mice, the expression levels of CD206 and CD163 were lower in OSMR$\beta^{-/-}$ mice (Fig. 6, *C* and *D*). These results indicate that OSMR$\beta^{-/-}$ mice exhibit adipose tissue inflammation under normal diet conditions.

To address the question of whether insulin resistance in OSMR$\beta^{-/-}$ mice resulted from inflammation in the adipose tissue, we treated OSMR$\beta^{-/-}$ mice with an anti-inflammatory agent, sodium salicylate. Both glucose intolerance and insulin resistance in OSMR$\beta^{-/-}$ mice were improved when the mice were treated with sodium salicylate (Fig. 6, *E–H*). These data suggest that inflammatory status in the adipose tissue is responsible for systemic insulin resistance of OSMR$\beta^{-/-}$ mice.

OSM Polarizes Macrophages to the M2 Phenotype—To investigate the effects of OSM on macrophage polarization, the expressions of several macrophage markers were determined in PEMs obtained from WT and OSMR$\beta^{-/-}$ mice. The expression of OSMRβ was observed in F4/80-positive cells in PEMs obtained from WT mice using flow cytometry (Fig. 7*A*). In addition, OSM activated STAT3 and CREB in PEMs obtained from WT mice but not in PEMs obtained from OSMR$\beta^{-/-}$ mice (Fig. 7*B*). Strikingly, the expressions of IL-10, MGL1, and MGL2 were markedly increased by OSM in PEMs obtained from WT mice (Fig. 7, *C–E*). In addition, OSM significantly increased the expression levels of arginase-1 and CD206 in

FIGURE 5. **Phenotypes of ATMs in WT and OSMR$\beta^{-/-}$ mice under normal diet conditions.** *A–F*, shown is expression of OSM and OSMRβ in the adipose tissue. *A*, shown is the mRNA expression of OSM in various tissues of C57BL/6J mice ($n = 6$). *B*, shown is mRNA expression of OSM in the SVF and adipocyte fraction in the adipose tissue of C57BL/6J mice ($n = 6$). *C*, shown is mRNA expression of OSM in the adipose tissue of WT and OSMR$\beta^{-/-}$ mice at 16 and 32 weeks of age ($n = 6$). *D*, shown is mRNA expression of OSMRβ in various tissues of C57BL/6J mice ($n = 6$). *E*, shown is mRNA expression of OSMRβ in the SVF and adipocyte fraction in the adipose tissue of C57BL/6J mice ($n = 6$). *F*, shown is immunofluorescence staining for OSMRβ (*red*) with F4/80 (*green*) and caveolin-1 (*blue*) in the adipose tissue of C57BL/6J mice. *Scale bars* = 100 μm. *G–I*, shown are the percentages (*G*) and total numbers (*H*) of F4/80-positive cells among the total numbers of cells in the SVF of the epididymal fat pads in WT and OSMR$\beta^{-/-}$ mice at 13, 16, and 32 weeks of age ($n = 4–6$). The total numbers of macrophages were normalized by the weights of the epididymal fat pads (*I*). *J* and *K*, shown are the percentages of CD11c-positive (*J*) and CD206-positive (*K*) cells in the F4/80-positive cells of WT and OSMR$\beta^{-/-}$ mice at 13, 16, and 32 weeks of age ($n = 4–6$). *L*, shown are the percentages of neutrophils (Gr-1^{high}/CD11b^{high} cells) in the total cells in the SVF of WT and OSMR$\beta^{-/-}$ mice at 13, 16, and 32 weeks of age ($n = 4–6$). The data represent the mean ± S.E. *, $p < 0.05$; **, $p < 0.01$ WT *versus* OSMR$\beta^{-/-}$ mice, Student's *t* test.

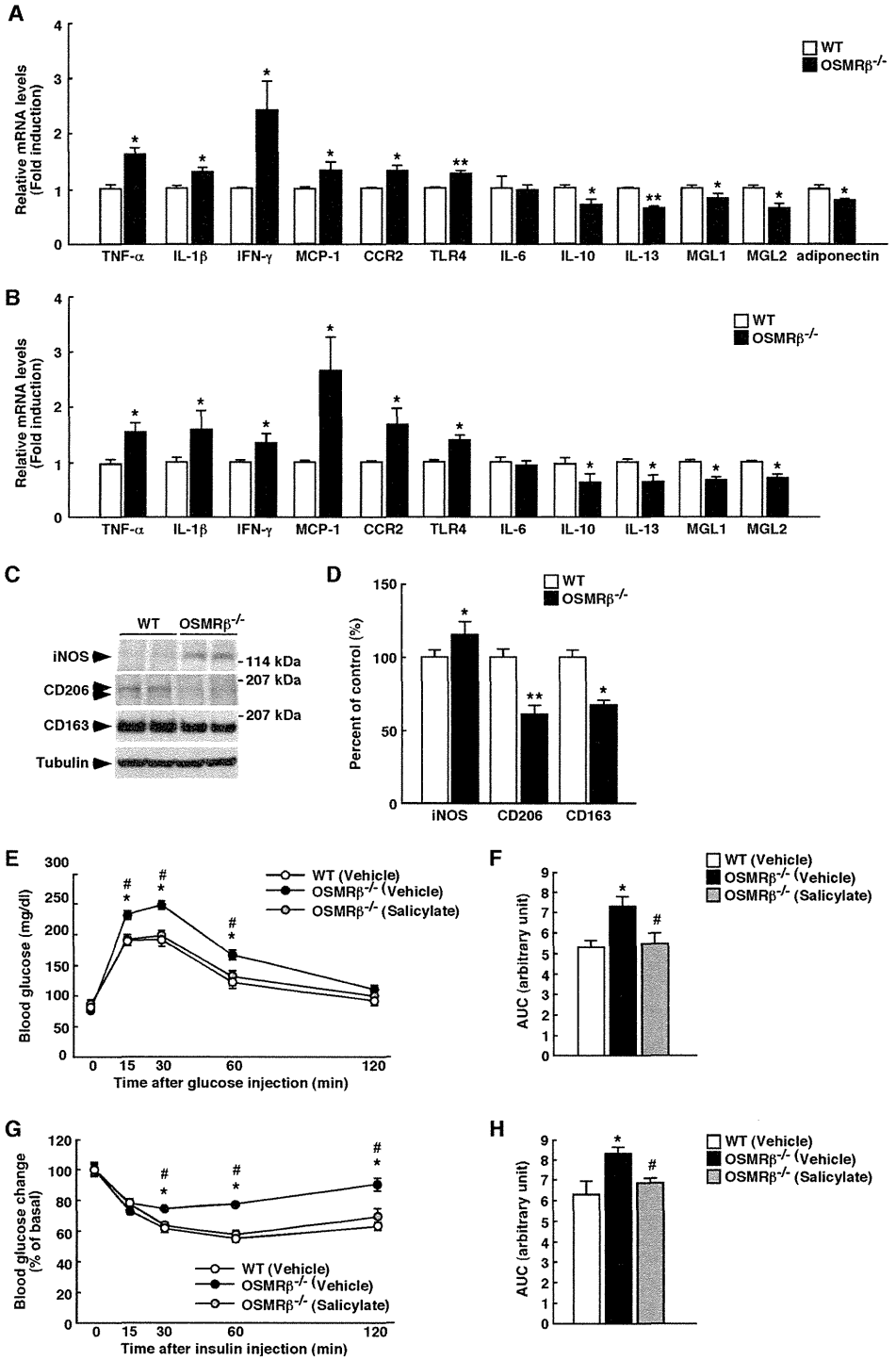

FIGURE 6. **Contribution of inflammatory status on insulin resistance in OSMR$\beta^{-/-}$ mice at 16 weeks of age.** *A* and *B*, shown are the expressions of proinflammatory markers (TNF-α, IL-1β, IFN-γ, MCP-1, CCR2, TLR4, and IL-6) and anti-inflammatory markers (IL-10, IL-13, MGL1, MGL2, and adiponectin) in the adipose tissue (*A*) and SVF (*B*) of WT and OSMR$\beta^{-/-}$ mice ($n = 6$). *C*, shown is Western blot analysis of markers of macrophage phenotypes (iNOS, CD206, and CD163) in the adipose tissue of WT and OSMR$\beta^{-/-}$ mice. The apparent molecular masses are indicated on the *right*. *D*, shown is quantitative analysis of the protein expression of iNOS, CD206, and CD163 ($n = 6$). *E–H*, shown are the effects of sodium salicylate on glucose intolerance and insulin resistance of OSMR$\beta^{-/-}$ mice. OSMR$\beta^{-/-}$ mice were injected intraperitoneally with either vehicle or sodium salicylate (120 μg/g body weight) once a day for 2 weeks. *E–H*, shown are the results of the ipGTTs (*E*) and ITTs (*G*) in OSMR$\beta^{-/-}$ mice injected with sodium salicylate. The areas under the curves (*AUC*) for blood glucose in the ipGTTs (*F*) and ITTs (*H*) are shown. The data represent the mean ± S.E. *, $p < 0.05$; **, $p < 0.01$ WT *versus* OSMR$\beta^{-/-}$ mice; #, $p < 0.05$ OSMR$\beta^{-/-}$ (*Vehicle*) *versus* OSMR$\beta^{-/-}$ (*Salicylate*) mice, ANOVA followed by the post-hoc Bonferroni test (*E* and *G*); Student's *t* test (*A*, *B*, *D*, *F*, and *H*).

PEMs obtained from WT mice (Fig. 7, *F* and *G*). The effects of OSM on the expressions of IL-10, MGL1, MGL2, arginase-1, and CD206 were completely abolished in PEMs obtained from OSMR$\beta^{-/-}$ mice (Fig. 7, *C–G*). The expression of iNOS, a marker of M1 macrophages, was not observed in PEMs regardless of whether the PEMs were

treated with OSM (Fig. 7*F*). In addition to that observed in PEMs, OSM induced the expressions of arginase-1 and CD206 in RAW264.7 cells, a mouse macrophage cell line (Fig. 7, *H* and *I*). OSM also increased the expressions of arginase-1 and CD206 and decreased the expression of iNOS in LPS-stimulated RAW264.7 cells (Fig. 7, *H* and *I*). Therefore, OSM can polarize the phenotypes of macrophages to M2.

OSM Polarizes ATMs to M2 Phenotype and Increases Insulin Sensitivity in Vivo—To investigate the effects of OSM on insulin sensitivity and phenotypic changes of ATMs, we treated

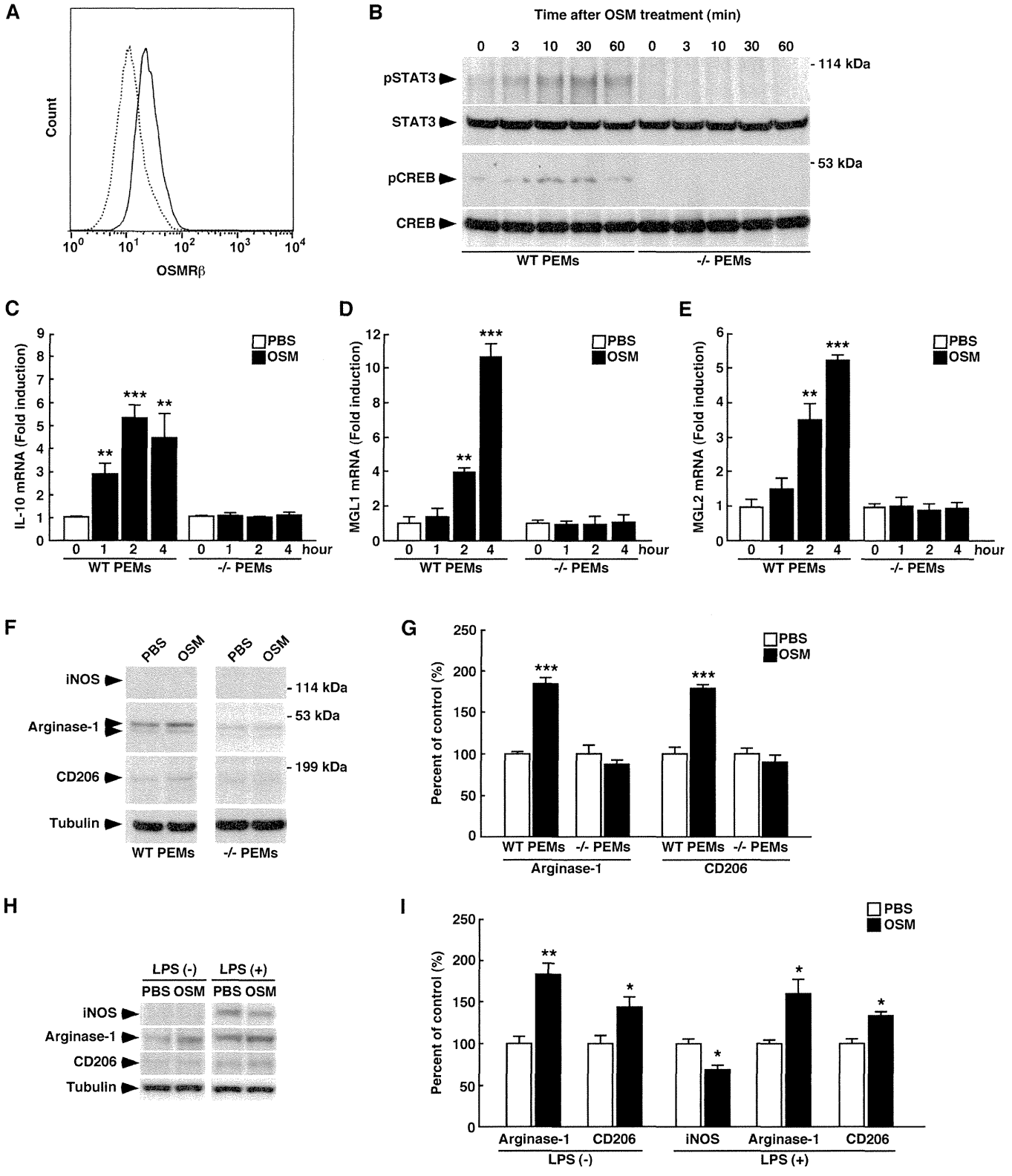

C57BL/6J mice with OSM for 1 week. Both glucose tolerance and insulin sensitivity in C57BL/6J mice were increased when the mice were treated with OSM (Fig. 8, *A–D*). In addition, both percentages and total numbers of F4/80-positive cells were reduced in mice treated with OSM (Fig. 8, *E–G*). The treatment with OSM increased the percentage of M2 ATMs but decreased the percentage of M1 ATMs in the adipose tissue (Fig. 8, *H* and *I*). In addition, OSM increased the expression of IL-10, IL-13, MGL1, and MGL2 in the adipose tissue (Fig. 8*J*). These data suggest that OSM can change the phenotypes of ATMs to M2 and increase insulin sensitivity *in vivo*.

DISCUSSION

OSM belongs to the IL-6 family of cytokines, including IL-6, IL-11, leukemia inhibitory factor, ciliary neurotrophic factor, and cardiotrophin-1 (30) and exhibits a variety of physiological functions, including the development of neurons and hepatocytes, hematopoiesis, and the modulation of inflammatory responses (21, 31–33). Although some members in this family, IL-6, ciliary neurotrophic factor, and cardiotrophin-1, are known to be associated with the development of obesity and insulin resistance (34–36), the role of OSM in these metabolic disturbances remains unclear. In this paper we have addressed this question using OSMR$\beta^{-/-}$ mice. OSMR$\beta^{-/-}$ mice exhibited obesity and insulin resistance at 32 weeks of age. Interestingly, insulin resistance preceding obesity was already observed in OSMR$\beta^{-/-}$ mice at 16 weeks of age.

It is well established that the balance between pro- and anti-inflammatory cytokines secreted from the adipose tissue is important for systemic insulin sensitivity. Proinflammatory cytokines, including TNF-α, IL-1β, and IFN-γ, promote the development of insulin resistance (16, 17, 37–40), whereas an anti-inflammatory cytokine, IL-10, improves obesity-induced insulin resistance (18). In the adipose tissue, these pro- and anti-inflammatory cytokines are produced by M1 and M2 macrophages, respectively (15). In the present study we found that the percentage of M1 macrophages and the expression of proinflammatory cytokines were increased in the adipose tissue of OSMR$\beta^{-/-}$ mice compared with WT mice. In contrast, the percentage of M2 macrophages and the expression of IL-10 were reduced in the adipose tissue of OSMR$\beta^{-/-}$ mice. Treatment of OSMR$\beta^{-/-}$ mice with sodium salicylate improved their insulin resistance, suggesting that systemic inflammation is important for the development of insulin resistance in OSMR$\beta^{-/-}$ mice. In addition, OSM was shown to directly polarize the phenotype of PEMs and RAW264.7 cells to M2. Furthermore, insulin sensitivity and the percentage of M2 ATMs were increased by the treatment with OSM *in vivo*. These findings suggest that OSM plays an important role in the regulation of energy homeostasis by insulin at least in part through the regulation of M1/M2 balance. In addition, Gr-1^{high}/CD11b^{high} cells, which are considered to be activated neutrophils, increased in the adipose tissue of OSMR$\beta^{-/-}$ mice. The increase of Gr-1^{high}/CD11b^{high} cells may contribute to drive or sustain the adipose tissue inflammation in OSMR$\beta^{-/-}$ mice.

As OSM is known to inhibit the differentiation of preadipocytes to mature adipocytes *in vitro* (41), our initial hypothesis was that OSM might reduce adiposity. However, there were no differences in the weight of adipose tissue between WT and OSMR$\beta^{-/-}$ mice under normal diet conditions. Most of the OSMRβ-positive cells were F4/80-positive macrophages, and few Dlk-1-positive preadipocytes were found in the adipose tissue. Furthermore, the phenotypes of the ATMs were polarized from M2 to M1 in OSMR$\beta^{-/-}$ mice fed a normal diet. These results suggest that macrophages play a more important role in the regulation of energy metabolism by OSM than do preadipocytes under normal diet conditions.

IL-6 potentially acts as a proinflammatory cytokine and induces hepatic insulin resistance in rodents (42, 43). However, chronic treatment of mice with IL-6 does not affect the insulin signaling in the skeletal muscle (42). In addition, IL-6-deficient mice showed systemic insulin resistance (34, 44). Therefore, the role of IL-6 in the development of systemic insulin resistance is controversial. In the present study, the IL-6 levels did not change in the adipose tissue of OSMR$\beta^{-/-}$ mice compared with those observed in the controls at 16 weeks of age when systemic insulin resistance developed in OSMR$\beta^{-/-}$ mice. By contrast, some proinflammatory cytokines (TNF-α, IL-1β, and IFN-γ), known to contribute to the development of insulin resistance (16, 17, 37–40), was significantly increased in the adipose tissue of OSMR$\beta^{-/-}$ mice. Therefore, IL-6 may function in the development of adipose tissue inflammation and insulin resistance in a manner distinct from that exhibited by other proinflammatory cytokines, including TNF-α, IL-1β, and IFN-γ. These observations suggest that our mouse model of metabolic syndrome with different expression patterns of proinflammatory cytokines may help in understanding functional differences between IL-6 and other proinflammatory cytokines in adipose tissue inflammation and insulin resistance.

The food intake is regulated by the hypothalamus and other associated regions of the brain, including the mesolimbic region and the brain stem (45). It has been reported that OSMRβ is expressed in a hypothalamic neuronal cell line, Gnv-4 cells (46). This finding raises the possibility that OSM

FIGURE 7. **The functional roles of OSM in macrophage.** *A*, shown is the expression of OSMRβ in PEMs obtained from WT mice. PEMs obtained from WT mice were stained with OSMRβ (*solid line*) or its control (*dotted line*) and analyzed by flow cytometry. *B*, shown is the activation of STAT3 and CREB by OSM in PEMs obtained from WT and OSMR$\beta^{-/-}$ mice. Western blot analysis of pSTAT3 and pCREB was performed in OSM-treated PEMs. The apparent molecular masses are indicated on the *right*. *C–E*, shown is the induction of IL-10 (*C*), MGL1 (*D*), and MGL2 (*E*) expression by OSM in PEMs. Quantitative real-time PCR was performed using mRNA prepared from OSM-treated PEMs obtained from WT and OSMR$\beta^{-/-}$ mice. *F*, shown are Western blot analyses of markers of macrophage phenotypes (iNOS, arginase-1, and CD206) in the OSM-treated PEMs obtained from WT and OSMR$\beta^{-/-}$ mice. The apparent molecular masses are indicated on the *right*. *G*, shown is quantitative analysis of the protein expression of arginase-1 and CD206. *H* and *I*, shown are the roles of OSM in RAW264.7 macrophages. *H*, shown is a Western blot analysis of markers of macrophage phenotypes (iNOS, arginase-1, and CD206) in non-stimulated or LPS-stimulated RAW264.7 macrophages. *I*, shown is a quantitative analysis of the protein expressions of iNOS, arginase-1, and CD206. The data represent the mean ± S.E. of three independent experiments. The data are expressed as percentages of control values (*white bars*). *, $p < 0.05$; **, $p < 0.01$; ***, $p < 0.005$ *versus* control, ANOVA followed by the post-hoc Bonferroni test (*C–E*); Student's *t* test (*G* and *I*).

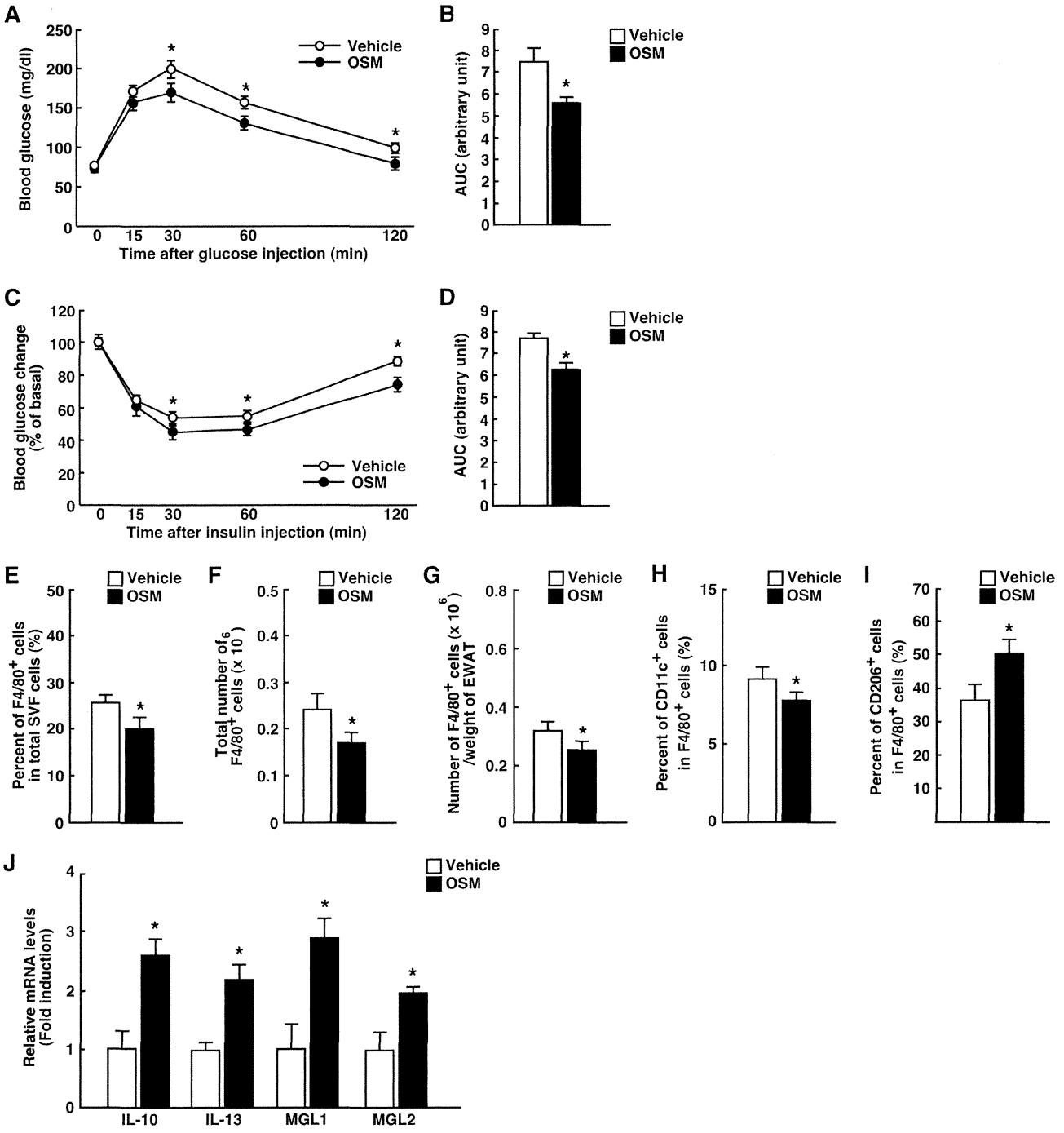

FIGURE 8. **Effects of OSM on phenotypes of ATMs and insulin sensitivity.** C57BL/6J mice were injected intraperitoneally with either vehicle or recombinant mouse OSM (12.5 ng/g body weight) twice a day for 1 week. *A–D*, shown are the results of the ipGTTs (*A*) and ITTs (*C*) in C57BL/6J mice injected with OSM (n = 4). The areas under the curves (*AUC*) for blood glucose in the ipGTTs (*B*) and ITTs (*D*) are shown. *E–G*, shown are the percentages (*E*) and total numbers (*F*) of F4/80-positive cells among the total numbers of cells in the SVF of the epididymal fat pads in C57BL/6J mice injected with OSM (n = 4). The total numbers of macrophages were normalized by the weights of the epididymal fat pads (*G*). *H* and *I*, shown are the percentages of CD11c-positive (*H*) and CD206-positive (*I*) cells in the F4/80-positive cells of C57BL/6J mice injected with OSM (n = 4). *J*, shown are the expressions of anti-inflammatory markers (IL-10, IL-13, MGL1, and MGL2) in the adipose tissue of C57BL/6J mice injected with OSM (n = 4). The data represent the mean ± S.E. *, $p < 0.05$ vehicle *versus* OSM, ANOVA followed by the post-hoc Bonferroni test (*A* and *C*); Student's *t* test (*B*, *D*, and *E–J*).

regulates food intake through the hypothalamus. However, we reported previously that OSMRβ is expressed only in the astrocytes of the olfactory bulb, the epithelial cells of the choroid plexus, and meningeal cells and not in the brain regions associated with food intake in normal adult mice (47). In addition, there were no significant differences in the food intake between WT and OSMRβ$^{-/-}$ mice fed a normal diet at 16 weeks of age, suggesting that OSM signaling is unlikely to regulate food intake under the normal conditions.

It has been most widely accepted that obesity is a major risk factor for the development of insulin resistance (1), which is followed by hyperinsulinemia, the exhaustion of pancreatic β

cells, and then the development of type 2 diabetes. However, there are also some reports inconsistent with this obesity-induced model of the pathogenesis of type 2 diabetes in human; that is, insulin resistance without obesity or hyperinsulinemia preceding obesity (48, 49). Thus, the relationship between obesity, insulin resistance, and type 2 diabetes remains unclear yet. In addition, there are few reports in the mouse model that insulin resistance occurs preceding obesity. Although insulin resistance without obesity is observed in the mice deficient in insulin or insulin signaling genes, including Akt2, these mice do not exhibit systemic inflammation (50, 51). As systemic inflammation, hyperinsulinemia, and insulin resistance preceded obesity in OSMR$\beta^{-/-}$ mice, OSMR$\beta^{-/-}$ mice constitute a unique mouse model of metabolic diseases and may help to clarify a novel relationship among systemic inflammation, hyperinsulinemia, insulin resistance, and obesity.

REFERENCES

1. Després, J. P., and Lemieux, I. (2006) Abdominal obesity and metabolic syndrome. *Nature* **444,** 881–887
2. Elgazar-Carmon, V., Rudich, A., Hadad, N., and Levy, R. (2008) Neutrophils transiently infiltrate intra-abdominal fat early in the course of high-fat feeding. *J. Lipid Res.* **49,** 1894–1903
3. Talukdar, S., Oh da, Y., Bandyopadhyay, G., Li, D., Xu, J., McNelis, J., Lu, M., Li, P., Yan, Q., Zhu, Y., Ofrecio, J., Lin, M., Brenner, M. B., and Olefsky, J. M. (2012) Neutrophils mediate insulin resistance in mice fed a high-fat diet through secreted elastase. *Nat. Med.* **18,** 1407–1412
4. Lumeng, C. N., Maillard, I., and Saltiel, A. R. (2009) T-ing up inflammation in fat. *Nat. Med.* **15,** 846–847
5. Weisberg, S. P., McCann, D., Desai, M., Rosenbaum, M., Leibel, R. L., and Ferrante, A. W. Jr. (2003) Obesity is associated with macrophage accumulation in adipose tissue. *J. Clin. Invest.* **112,** 1796–1808
6. Hirasaka, K., Kohno, S., Goto, J., Furochi, H., Mawatari, K., Harada, N., Hosaka, T., Nakaya, Y., Ishidoh, K., Obata, T., Ebina, Y., Gu, H., Takeda, S., Kishi, K., and Nikawa, T. (2007) Deficiency of Cbl-b gene enhances infiltration and activation of macrophages in adipose tissue and causes peripheral insulin resistance in mice. *Diabetes* **56,** 2511–2522
7. Kanda, H., Tateya, S., Tamori, Y., Kotani, K., Hiasa, K., Kitazawa, R., Kitazawa, S., Miyachi, H., Maeda, S., Egashira, K., and Kasuga, M. (2006) MCP-1 contributes to macrophage infiltration into adipose tissue, insulin resistance, and hepatic steatosis in obesity. *J. Clin. Invest.* **116,** 1494–1505
8. Lesniewski, L. A., Hosch, S. E., Neels, J. G., de Luca, C., Pashmforoush, M., Lumeng, C. N., Chiang, S. H., Scadeng, M., Saltiel, A. R., and Olefsky J. M. (2007) Bone marrow-specific Cap gene deletion protects against high-fat diet-induced insulin resistance. *Nat. Med.* **13,** 455–462
9. Weisberg, S. P., Hunter, D., Huber, R., Lemieux, J., Slaymaker, S., Vaddi, K., Charo, I., Leibel, R. L., and Ferrante, A. W. Jr. (2006) CCR2 modulates inflammatory and metabolic effects of high-fat feeding. *J. Clin. Invest.* **116,** 115–124
10. Hamilton, T. A. (2002) in *The Macrophage* (Bourke, B., and Lewis, C. eds) pp. 73–102, Oxford University Press, Oxford
11. Gordon, S. (2003) Alternative activation of macrophages. *Nat. Rev. Immunol.* **3,** 23–35
12. Modolell, M., Corraliza, I. M., Link, F., Soler, G., and Eichmann, K. (1995) Reciprocal regulation of the nitric oxide synthase/arginase balance in mouse bone marrow-derived macrophages by TH1 and TH2 cytokines. *Eur. J. Immunol.* **25,** 1101–1104
13. Munder, M., Eichmann, K., and Modolell, M. (1998) Alternative metabolic states in murine macrophages reflected by the nitric oxide synthase/arginase balance. Competitive regulation by CD4+ T cells correlates with Th1/Th2 phenotype. *J. Immunol.* **160,** 5347–5354
14. Lumeng, C. N., Bodzin, J. L., and Saltiel, A. R. (2007) Obesity induces a phenotypic switch in adipose tissue macrophage polarization. *J. Clin. Invest.* **117,** 175–184
15. Fujisaka, S., Usui, I., Bukhari, A., Ikutani, M., Oya, T., Kanatani, Y., Tsuneyama, K., Nagai, Y., Takatsu, K., Urakaze, M., Kobayashi, M., and Tobe, K. (2009) Regulatory mechanisms for adipose tissue M1 and M2 macrophages in diet-induced obese mice. *Diabetes* **58,** 2574–2582
16. de Alvaro, C., Teruel, T., Hernandez, R., and Lorenzo, M. (2004) Tumor necrosis factor-α produces insulin resistance in skeletal muscle by activation of inhibitor κB kinase in a p38 MAPK-dependent manner. *J. Biol. Chem.* **279,** 17070–17078
17. Nguyen, M. T., Satoh, H., Favelyukis, S., Babendure, J. L., Imamura, T., Sbodio, J. I., Zalevsky, J., Dahiyat, B. I., Chi, N. W., and Olefsky, J. M. (2005) JNK and tumor necrosis factor-α mediate free fatty acid-induced insulin resistance in 3T3-L1 adipocytes. *J. Biol. Chem.* **280,** 35361–35371
18. Hong, E. G., Ko, H. J., Cho, Y. R., Kim, H. J., Ma, Z., Yu, T. Y., Friedline, R. H., Kurt-Jones, E., Finberg, R., Fischer, M. A., Granger, E. L., Norbury, C. C., Hauschka, S. D., Philbrick, W. M., Lee, C. G., Elias, J. A., and Kim, J. K. (2009) Interleukin-10 prevents diet-induced insulin resistance by attenuating macrophage and cytokine response in skeletal muscle. *Diabetes* **58,** 2525–2535
19. Tanaka, M., Hara, T., Copeland, N. G., Gilbert, D. J., Jenkins, N. A., and Miyajima, A. (1999) Reconstitution of the functional mouse oncostatin M (OSM) receptor. Molecular cloning of the mouse OSM receptor β subunit. *Blood* **93,** 804–815
20. Tamura, S., Morikawa, Y., Miyajima, A., and Senba, E. (2002) Expression of oncostatin M in hematopoietic organs. *Dev. Dyn.* **225,** 327–331
21. Wallace, P. M., MacMaster, J. F., Rouleau, K. A., Brown, T. J., Loy, J. K., Donaldson, K. L., and Wahl, A. F. (1999) Regulation of inflammatory responses by oncostatin M. *J. Immunol.* **162,** 5547–5555
22. Dillon, S. R., Sprecher, C., Hammond, A., Bilsborough, J., Rosenfeld-Franklin, M., Presnell, S. R., Haugen, H. S., Maurer, M., Harder, B., Johnston, J., Bort, S., Mudri, S., Kuijper, J. L., Bukowski, T., Shea, P., Dong, D. L., Dasovich, M., Grant, F. J., Lockwood, L., Levin, S. D., LeCiel, C., Waggie, K., Day, H., Topouzis, S., Kramer, J., Kuestner, R., Chen, Z., Foster, D., Parrish-Novak, J., and Gross, J. A. (2004) Interleukin 31, a cytokine produced by activated T cells, induces dermatitis in mice. *Nat. Immunol.* **5,** 752–760
23. Tanaka, M., Hirabayashi, Y., Sekiguchi, T., Inoue, T., Katsuki, M., and Miyajima, A. (2003) Targeted disruption of oncostatin M receptor results in altered hematopoiesis. *Blood* **102,** 3154–3162
24. Morikawa, Y., Furotani, M., Matsuura, N., and Kakudo, K. (1993) The role of antigen-presenting cells in the regulation of delayed-type hypersensitivity. II. Epidermal Langerhans' cells and peritoneal exudate macrophages. *Cell. Immunol.* **152,** 200–210
25. Komori, T., Doi, A., Furuta, H., Wakao, H., Nakao, N., Nakazato, M., Nanjo, K., Senba, E., and Morikawa, Y. (2010) Regulation of ghrelin signaling by a leptin-induced gene, negative regulatory element-binding protein, in the hypothalamic neurons. *J. Biol. Chem.* **285,** 37884–37894
26. Komori, T., Gyobu, H., Ueno, H., Kitamura, T., Senba, E., and Morikawa, Y. (2008) Expression of kin of irregular chiasm-like 3/mKirre in proprioceptive neurons of the dorsal root ganglia and its interaction with nephrin in muscle spindles. *J. Comp. Neurol.* **511,** 92–108
27. Lumeng, C. N., DelProposto, J. B., Westcott, D. J., and Saltiel, A. R. (2008) Phenotypic switching of adipose tissue macrophages with obesity is generated by spatiotemporal differences in macrophage subtypes. *Diabetes* **57,** 3239–3246
28. Komori, T., Morikawa, Y., Tamura, S., Doi, A., Nanjo, K., and Senba, E. (2005) Subcellular localization of glucose transporter 4 in the hypothalamic arcuate nucleus of ob/ob mice under basal conditions. *Brain Res.* **1049,** 34–42
29. Folch, J., Lees, M., and Sloane Stanley, G. H. (1957) A simple method for the isolation and purification of total lipides from animal tissues. *J. Biol. Chem.* **226,** 497–509
30. Taga, T., and Kishimoto, T. (1997) Gp130 and the interleukin-6 family of cytokines. *Annu. Rev. Immunol.* **15,** 797–819
31. Kamiya, A., Kinoshita, T., Ito, Y., Matsui, T., Morikawa, Y., Senba, E., Nakashima, K., Taga, T., Yoshida, K., Kishimoto, T., and Miyajima, A. (1999) Fetal liver development requires a paracrine action of oncostatin M through the gp130 signal transducer. *EMBO J.* **18,** 2127–2136
32. Morikawa, Y., Tamura, S., Minehata, K., Donovan, P. J., Miyajima, A., and Senba, E. (2004) Essential function of oncostatin m in nociceptive neurons